Automatic and Robust Technique for Segmentation and Classification of Acute Lymphoblastic Leukemia using Adaptive Multi-Dilated Residual Attention Network and Heuristic Strategy

Abirami M.[1,*], Victo Sudha George G.[2] , Dahlia Sam S.[1]

[1]Department of Information Technology, Dr.M.G.R. Educational and Research Institute

[2]Department of Computer Science and Engineering, Dr.M.G.R. Educational and Research Institute

Emails: abiprj@gmail.com; victosudhageorge@drmgrdu.ac.in; dahliasam@drmgrdu.ac.in

Abstract

Leukemia is a very dangerous kind of malignancy troubling the blood or bone marrow in all age categories, both in adults and children. The deadly and threatening kind of leukemia is named Acute Lymphoblastic Leukemia (ALL). The accurate and automated ALL diagnosis of blood cancer is complex work. Medical experts and hematologists in the bone marrow and blood samples detect it by employing a high-quality microscope. The manual classification is observed as tiresome and is restricted by varying expert considerations and other attributes. Presently, the Convolutional Neural Networks (CNNs) have become an acceptable mechanism for analyzing the medical image. However, for attaining outstanding performance, conventional CNNs normally demand large data sources for better training. Thus, to alleviate the existing complexities, we implemented an effective ALL detection system using deep learning. At first, the necessitated images are aggregated from global resources of data. Further, the garnered images are inputted into the Optimized Trans-Res-Unet+ (OTRUnet+)-based segmentation model. Here, the Fitness-aided Position Updating in the Social engineering Algorithm (FPUSA) for improving the segmentation process's efficacy optimally tunes the OTRUnet+ technique parameters. In addition, the segmented images are taken to perform the classification process using the Adaptive Multi-Dilated Residual Attention Network (AMDRAN); here several parameters are optimally tuned by the same FPUSA to enrich the classification process. Finally, the suggested AMDRAN technique offered the ALL classified output. The effectiveness of the designed ALL detection system is explored with several existing systems to display its enhanced performance over other models

Keywords: Acute Lymphoblastic Leukemia; Segmentation and Classification; Optimized Trans-Res-Unet+; Adaptive Multi-Dilated Residual Attention Network; Fitness-aided Position Updating in Social engineering Algorithm

1. Introduction

One of the blood cancer categories is leukemia that causes white blood cells (WBCs) of the body to become malignant. The immune system of the body is placed at risk by the cancerous cells that trouble the blood and bone marrow and it suppresses the generation of the platelet and red blood cells in the bone marrow [9]. Based on the affected WBCs, leukemia is categorized into two categories: if the affected white cells are granulocytes or monocytes, then Acute Myeloid Leukemia (AML) or myelogeneous or if the affected white cells are lymphocytes then ALL or lymphoblastic [10]. ALL is defined as the dangerous hematological situation classified by the overproduction and started extension of immature and cancerous WBCs. The disorder can cause death if left uncured. Here, the blasts quickly propagate into vital organs and bloodstream [11]. Therefore, to raise the level of recovery and treatment, the impairment must be detected quickly. The whole is usually identified using a global blood count test based on WBC count [12]. Aspiration by the bone marrow, microscopy of blood smears is used to ensure that individuals have been detected by leukemia. However, these manual identification strategies are both expensive and tiresome. Considering the various drawbacks of manual

DOI: https://doi.org/10.54216/FPA.190217
Received: January 11, 2025 Revised: February 18, 2025 Accepted: March 06, 2025

identification techniques, the diagnostic and computer-aided identification approaches employing deep learning are a significant alternative [13]. The computer-assisted techniques have been confirmed to be cost-effective, correct, fast, and efficient contrasted to the conventional mechanisms.

Leukocytes, often known as white blood cells, are typically found in approximately 1% of total blood cells. It is found in bone marrow, blood, and extramedullary locations. This type of leukemia necessitates prompt detection because the immature leukocytes spread swiftly throughout the body. Generally, the detection is carried out based on bone marrow text. This approach is tiresome, labour intensive, and may produce inaccurate outcomes. Hence, there is a requirement for automation [14]. Machine learning, deep learning processes, and computer vision-aided techniques are used in contemporary experimental investigations to quickly identify ALL from microscopic images. The diagnosis of ALL is significantly influenced by the nucleus of the WBC segmentation. The leukemia cells are identified by segmenting the blood cells using the least squares-aided geometric elliptical fitting mechanism. The k-means approach and color space conversion-aided segmentation approaches of WBC's nucleus and Convolutional Neural Network (CNN) technique-aided classification have been adopted [15]. In the past decades, active contour approaches, watershed methods, region-aided segmentation, cluster-aided segmentation, and neural network-assisted segmentation have been employed [16]. Sometimes, these techniques are tiresome and generate very poor segmentation outcomes. In the modern years, various Artificial Intelligence (AI)-aided segmentation techniques have integrated deep learning with CNNs, allowing the implementation of potential computer devices for healthcare assistance [17]. The neural networks must be trained and tuned to perform the required function, however, which requires a significant quantity of data and computing power.

Though the automation in ALL diagnosis is significant in all kinds of cancer classification, it is complex because of the morphological correlation among normal and cancerous cells [18]. The conventional ALL diagnosis mechanism requires experienced medical experts to analyze the cell images carefully that is tiresome, arduous, and most of the time affects variations of inter-observer. Nowadays, deep learning mechanisms have attained popularity due to these mechanisms can understand the significant features via rigorous training. The machine learning's subset is deep learning that concentrates to move the conventional machine learning mechanisms towards AI. Deep learning prevents the limitations of feature engineering, and machine learning subset techniques that, by extracting the features automatically from the image and enhancing the accuracy of the system make it possible to resolve complex issues to high extents. However, these methods comprehend the characteristics of the provided data.Furthermore, the essential selection of associated hyper-parameter training, which can significantly affect classification functionality, is not examined by conventional methods.

The contributions of the designed ALL classification system are provided below.

- ♣ To suggest a novel framework for ALL classification by incorporating the deep learning strategies and improved version of optimization that accurately provides the ALL classified outcomes for supporting the medical experts to cure the individuals in the correct time.
- ♣ To present the OTRUnet+ technique by integrating the transformer and ResUnet+ tasks that segment the image abnormalities and assist the classification process. Here, the FPUSA is employed for optimizing the OTRUnet+ technique parameters. It increases the accuracy and dice coefficient of the model.
- ♣ To construct the AMDRAN approach by combining the multi-dilated mechanism and RAN technique that performs the ALL classification effectively. Here, the FPUSA is utilized to optimally tune the parameters of the AMDRAN approach. This minimizes the error rates of the classification process.
- ♣ To build the new FPUSA by adopting the existing SEO that highly aids to optimally determines the parameters of OTRUnet+ and AMDRAN techniques thus improving the functionality rates and accuracy of the overall ALL diagnosis process.
- ♣ To examine the effectualness of the suggested ALL classification system by adopting several traditional mechanisms and algorithms that display the robustness and uniqueness of the designed system.

The designed ALL classification technique is constructed by the following parts. Part II explains the existing research on the ALL classification process. Part III elaborates on the segmentation and classification of ALL: proposed work and image acquisition. Part IV describes the abnormality segmentation using OTRUnet+ for ALL diagnoses. Part V elucidates the disease detection with AMDRAN and its objective function. Part VI displays the results and justifications of the presented ALL detection. Part VII concludes the ALL diagnosis work with its future work.

DOI: https://doi.org/10.54216/FPA.190217
Received: January 11, 2025 Revised: February 18, 2025 Accepted: March 06, 2025

2. Existing Works

2.1 Related Works

In 2023, Resendiz *et al.* [1] have recommended a framework based on deep learning for diagnosing ALL that offered interpretable and reliable classification. The objective was to implement an automatic model that could support medical experts in detecting leukemia very effectively, relatively enhancing patient outcomes. The experiment findings provided reliable solutions.

In 2021, Alagu *et al.* [2] have suggested the significant features for identifying the ALL. The necessary images were aggregated from public data sources. The achieved images were resized and various significant features were extracted. At last, the statistical evaluation was conducted and the functionality of the model was validated. It was identified that the features were highly suitable to recognize the ALL. In 2020, Anwar and Alam [3] have offered an automated model to recognize the ALL-employing CNN. The system employed numerous data augmentation mechanisms to improve the amount of training information and minimize the over-training issue. The system did not require segmentation or pre-processing mechanisms and performed effectively on original data.

In 2022, Sampathila *et al.* [4] have introduced a novel mechanism to analyze the WBCs and to support the timely identification of ALL. The task employed CNN to forecast the leukemic cells from ordinary blood cells. The technique was trained on a standard database and attained higher sensitivity and accuracy.

In 2024, Saeed *et al.* [5] have explored an automated model for detecting the ALL disorder employing CNN techniques. The data augmentation mechanisms have been adopted to produce the images to rectify the overfitting issue in the technique. Qualitative evaluation has been conducted and the outcomes displayed that the author's model achieved higher accuracy in the diagnosis of ALL.

In 2022, Jawahar *et al.* [6] have offered a Deep Neural Network (DNN) technique that supported to categorize the WBC images. The work extracted the wide and local attributes from the given images for the effective ALL prediction. The functionality of the system was contrasted with various classical mechanisms. The outcomes displayed that the model produced a higher f1-score and accuracy.

2.2 Research Gaps and Challenges

An ALL in the human white cells is dangerous and demands quick medical treatments. It is a fatal kind of disease that causes high death rates among adults and children. Medical experts attain conventional diagnosis of this disorder via evaluating the WBC's microscopic images. However, this strategy depends on manual observation and offers inaccurate outcomes. Hence, automatic ALL diagnosis techniques have been implemented in the past years. But, the existing ALL diagnosis mechanisms face some imitations including high computational complexity, high error rates, long execution time, and so on. Table I depicts the advantages and challenges of existing ALL diagnosis techniques and the primary challenges of the existing models are listed as follows.

- The classification of ALL is a hot topic nowadays in the medical sector. However, the manual diagnosis techniques are prone to error, hence demanding automatic ALL diagnosis techniques. Though there are numerous automatic ALL diagnosis techniques, these techniques still require many improvements in terms of computational resource utilization, time execution, computational cost, etc. By considering these factors an effective ALL, segmentation and classification approach is implemented in this work.
- Most of the existing ALL segmentation techniques fail to segment and locate the abnormalities effectively. Moreover, the traditional techniques did not consider the tiny regions while segmenting the abnormalities. This may affect the final classification process. Thus, this work introduces a very effective segmentation technique based on deep learning that accurately segments the abnormalities even if the location is very tiny.
- However, various classical ALL classification models offer accurate outcomes these techniques did not perform well in large-scale datasets and face numerous issues such as overfitting and the curse of dimensionality. Thus, a novel classification mechanism is presented in this work for categorizing the ALL.
- The traditional ALL diagnosis approaches did not perform the parameter optimization for both segmentation and classification tasks. Mostly, the traditional techniques perform the parameter optimization in either the segmentation stage or classification stage. This may affect the effectiveness of the model. Therefore, a modified heuristic approach is invented in this work for optimizing the parameters of both segmentation and classification techniques.

DOI: https://doi.org/10.54216/FPA.190217
Received: January 11, 2025 Revised: February 18, 2025 Accepted: March 06, 2025

- Most of the traditional ALL diagnosis techniques provided inaccurate outcomes for both segmentation and classification tasks. Thus, this task introduces diverse powerful performance metrics to evaluate the designed model and contrast it with its traditional models. This proves the suggested model's efficacy over traditional techniques.

Thus, this work introduced an intelligent ALL segmentation and classification framework with the assistance of deep learning.

Table 1: Features and Challenges of Traditional ALL Classification Techniques

Author [citation]	**Methodology**	**Features**	**Challenges**
Resendiz *et al.* [1]	Unet	It accurately segments the complex images. It offers high performance rates and provides solutions rapidly.	It is computationally very complex. It could not realize the global semantic data interaction.
Alagu *et al.* [2]	AlexNet	It offers promising functionality rates. It leads to fast training and generates successful outcomes.	It has a high computational cost. Its inference time is too short.
Anwar and Alam [3]	CNN	It reduces the computations. It offers very accurate outcomes.	It is computationally very expensive. It takes a long training time.
Sampathila *et al.* [4]	ResNet	It rectifies the vanishing gradient issues. It is easy to optimize the network parameters.	It is prone to testing errors. It is very complex to train the network.
Saeed *et al.* [5]	CNN	It effectively manages the large-size data sources. It automatically realizes the rich features.	It demands vast labeled data. It faces interpretability limitations.
Jawahar *et al.* [6]	EfficientNetB3	It employs very less amount of parameters. It is an effective and rapid model.	It produces poor outcomes. It has dimensionality issues.
Zakir Ullah *et al.* [7]	CNN	It does not demand human intervention. It performs the hierarchical learning.	It is susceptible to overfitting. It is susceptible to adversarial threats.
Rodrigues *et al.* [8]	CNN	It discovers the salient features from the original images accurately. It performs well in complex images.	It faces class imbalance issues. It troubles to perform well in small datasets.

DOI: https://doi.org/10.54216/FPA.190217
Received: January 11, 2025 Revised: February 18, 2025 Accepted: March 06, 2025

3. Segmentation and Classification of Acute Lymphoblastic Leukemia Proposed Work and Image Acquisition

3.1 Image Acquisition

The requisite images for diagnosing the ALL are gathered from the following datasets.

Dataset 1("Acute Lymphoblastic Leukemia (ALL) image dataset"): This data source is obtained through the link "https://www.kaggle.com/datasets/mehradaria/leukemia: access date: 2024-04-24" from Kaggle. This dataset contains 3256 images from 89 predicted of ALL patients. This data source is classified into two malignant and non-cancerous. The cancerous lymphoblasts are subdivided into three such as Pro- B ALL, Early Pre-B, and Pre-B. The entire images are in JPG format.

Dataset 2("Acute Lymphoblastic Leukemia Dataset Image Dataset"): This data source is attained via a hyperlink "https://universe.roboflow.com/lucas-reis/acute-lymphoblastic-leukemia-dataset/dataset/10: access date: 2024-04-24". It includes 367 images, where 293 images are supported for the training set, 37 images are supported for the valid set and 37 images are supported for the test set.

From the above data sources, the garnered images are declared as A_l, *here* $l = 1,2,\ldots,L$ and the collected image's overall amount is specified as L . The sample images for the presented ALL process are given in Fig.1

Images	**1**	**2**	**3**	**4**	**5**
"Dataset 1"	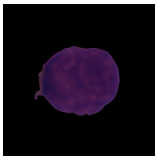	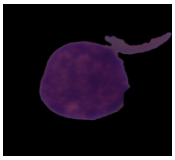	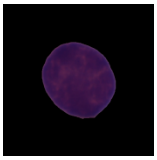	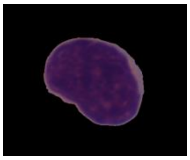	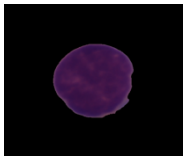
"Dataset 2"	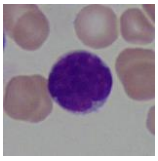	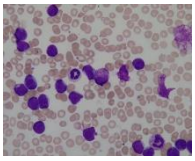	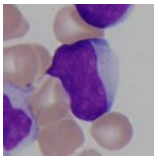	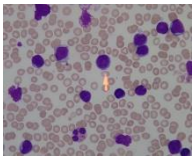	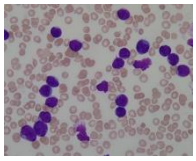

Figure 1. Sample images for recommended ALL diagnosis process

3.2 Illustration of Novel ALL Segmentation and Classification

Leukaemia is a haematological disorder featuring an abnormally huge amount of WBCs. The unusual WBCs are not entirely developed WBCs and hence perform very poorly in the immune system. ALL is one kind of leukemia that grows in the bone marrow and troubles lymphocyte cells. Distinct genetic mechanisms have been utilized for the malignancy of changing cells. However, if it is not recognized and treated at the proper time, it can grow quickly and take human life in a short period. Machine learning and deep learning methodologies are employed in the ALL detection task. However, the machine learning strategies highly rely on each stage's success; hence, the identification task is still not effective. The deep learning techniques that employ the feed-forward and back propagation of deep learning can generalize the illustrations of features in the blood's microscopic pictures. The attributes of the weights are extracted from the given images and the outcomes are categorized employing the final layer's activation function to connect among the actual class and the forecasting class. Numerous experts nowadays employ deep learning strategies to generate better technique performance than machine learning strategies concerning estimation factors in identifying the ALL. Categorizing and localizing the cells in the given images can support the medical experts make timely diagnoses and offer significant therapy to minimize the severity of the disease. However, traditional deep learning strategies encounter computational burdens, long execution periods, gradient issues, and so on. Thus, implementing an effective ALL diagnosis mechanism is significant. The recommended ALL diagnosis process's illustration is presented in Fig.1.

DOI: https://doi.org/10.54216/FPA.190217
Received: January 11, 2025 Revised: February 18, 2025 Accepted: March 06, 2025

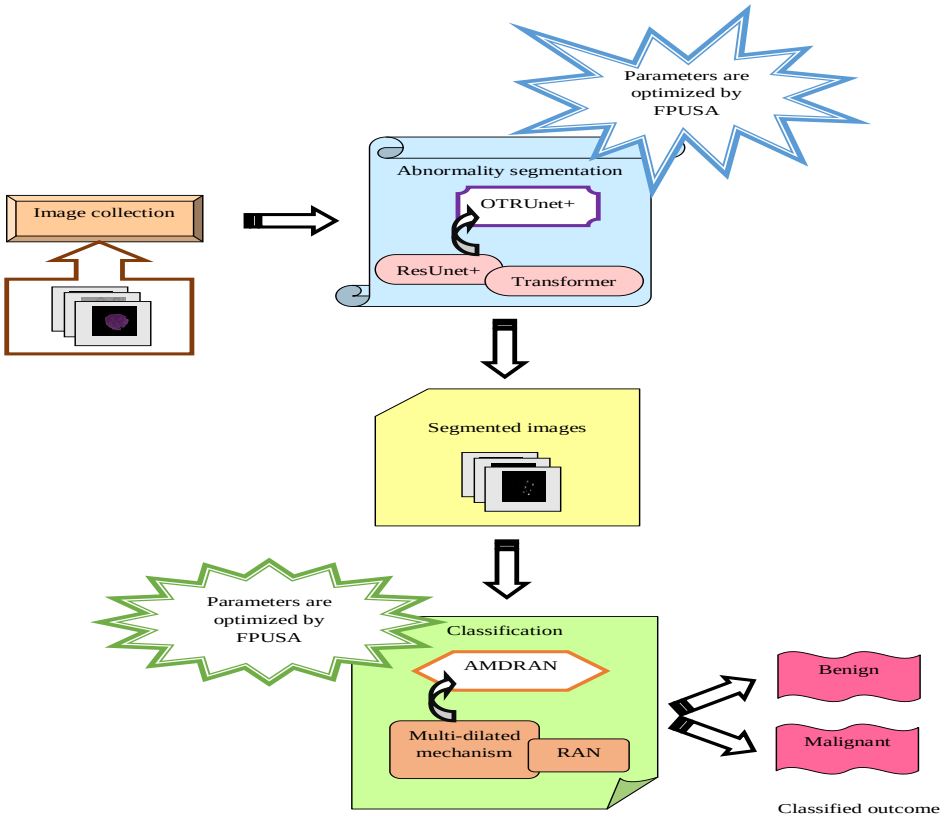

Figure 2. The architecture of the recommended ALL diagnosis process using deep learning strategies

An intelligent ALL diagnosis mechanism is offered in this work by incorporating the concept of deep learning. Initially, the required images are aggregated from the standard datasets. In addition, the images are forwarded to the OTRUnet+-based segmentation approach, where abnormalities are segmented accurately. In this operation, the FPUSA is recommended for improving the efficacy of the segmentation task. After that, the segmented images are preceded as input for the designed AMDRAN technique, where the ALL is classified. In this process also, the FPUSA is suggested for enhancing the performance status of the classification process by optimally tuning the AMDRAN parameters. Finally, the suggested ALL diagnosis process is validated and compared with the conventional techniques to portray the effectualness of the offered framework.

3.3 Parameter Tuning: FPUSA

The FPUSA is designed in this work to produce higher performance in the overall ALL segmentation and diagnosis process. Moreover, the designed FPUSA helps to optimize the parameters such as the counts of the hidden neuron, activation function, and count of epochs for both segmentation and classification techniques in ALL diagnosis processes.

Purpose: The FPUSA is implemented for optimizing the parameters of the OTRUnet+ technique such as "hidden neuron counts, steps per epoch, and a number of epochs". Moreover, the attributes such as "hidden neuron counts, activation function, and number of epochs" in the MDRAN technique are also optimized by the FPUSA approach. This technique is designed from the traditional SEO technique, where the solutions are obtained by utilizing the defender and attacker features. This algorithm resolves the multi-objective optimization issues and employs in real time applications. However, the traditional SEO employs the arbitrary distribution variable in the bound of 0 and 1 for performing each stage in the algorithm. When the iteration count increases, most of the time because of this random factor, the iteration takes more amount of time and also it is susceptible to inaccurate solutions. Hence, the FPUSA approach is introduced in this work by preventing the mentioned limitations.

Novelty: As mentioned already, the suggested FPUSA is designed from SEO to prevent the limitations of the traditional technique. In the designed FPUSA, the random variable in the conventional SEO is upgraded with the help of fitness variables. Thus, a new arbitrary factor is introduced to perform the tasks in FPUSA thus; it enhances the accuracy rates and decreases the execution time. The FPUSA technique's new arbitrary variable is mathematical expression is given in Eq. (1).

DOI: https://doi.org/10.54216/FPA.190217
Received: January 11, 2025 Revised: February 18, 2025 Accepted: March 06, 2025

$$\begin{aligned} &if \quad mfit > 1 \\ &\qquad Q = \frac{bfit}{(wfit * mfit * ft(m))} \\ &else \\ &\qquad Q = \frac{(wfit * mfit * ft(m))}{bfit} \end{aligned} \tag{1}$$

Here, the new random variable is declared as Q , and the mean fitness is declared as $mfit$. The best and worst fitness variables are pointed as $bfit$ *and* $wfit$ respectively. The variable $ft(m)$ is $fitness(m)$, *here* $m = 1,2,..,M_{pop}$. If the value of mean fitness is greater than one, then the random variable is upgraded based on $Q = \frac{bfit}{(wfit * mfit * ft(m))}$. Or else the new random variable is upgraded on the basis of $Q = \frac{(wfit * mfit * ft(m))}{bfit}$. Thus, the new arbitrary factor is involved in the FPUSA approach for searching and finding out the optimal solutions. This new upgraded arbitrary factor is employed from Eq. (5) to Eq. (9) for enhancing the performance. The SEO model's process is explained below.

The SEO [26] initiates with two primary outcomes partitioned into two including defender and attacker. The predator attains the conditions of social engineering mechanisms to meet its specific objectives.

Initialization: The objective of the optimizer is to discover the optimal outcome between all better outcomes. An array of attributes to be optimized is implemented. This array is formulated in Eq. (2).

$$pr = \lfloor S_1, S_2, S_3, ..., S_{M_{vr}} \rfloor \tag{2}$$

Here, the person is specified as pr and the variable $S_{M_{vr}}$ denotes the total count of persons.

In addition, the objective function value vl is determined for two members as given in Eq. (3).

$$vl = g(pr) = g(S_1, S_2, S_3 ...., S_{M_{vr}}) \tag{3}$$

Train and retrain: This phase concentrates to display the retraining and training of the attacker from the protector. Here, the β percent of predator traits are chosen arbitrarily and are exchanged in the similar protector's traits as in Eq. (4).

$$S_{Tr} = round(\beta.mVr) \tag{4}$$

Here, the percent of chosen traits is denoted as β , and the amount of total traits is indicated as mVr . The amount of traits is indicated as S_{Tr} that will be validated on the several arbitrary defender traits.

Spot on attack: In order to discover the attack, the SEO approach takes four distinct mechanisms including pretext, diversion, phishing, and obtaining. In all derivations, the variable de_{ne} is displayed as the defender's new place during the attack. The variables at *and* de_{ol} are the attacker and defender's present places accordingly.

i) ***Obtaining:*** In this mechanism, the attacker directly misuses the protector to achieve the specific goal. To generate the new place, Eq. (5) is recommended.

$$\begin{aligned} de_{ne} &= de_{ol} \times (1 - \sin \ \alpha \times Q) \\ &+ \frac{de_{ol} + at}{2} \times \sin \ \alpha \times Q \end{aligned} \tag{5}$$

This movement is according to the arbitrary distribution Q and the rate of discovering the attack is given as α . Traditional SEO employs the arbitrary distribution attribute in the boundary of 0 and 1 for the tasks. This random variable minimizes the correctness and increases the processing time. To mitigate these issues, with the aid of Eq. (1), a new arbitrary variable Q is invented and this enhanced random variable is utilized in the tasks of FPUSA.

ii) ***Phishing:*** To model this approach, the predator acts to mechanism the protector, and further the protector forwards to the region where the predator needs to be there.

DOI: https://doi.org/10.54216/FPA.190217
Received: January 11, 2025 Revised: February 18, 2025 Accepted: March 06, 2025

$$de_{ne}^{1} = at \times (1 - \sin\ \alpha) \times Q + \frac{(de_{ol} + at)}{2} \times \sin\ \alpha \times Q \quad (6)$$

$$de_{ne}^{2} = de_{ol} \times \left(1 - \sin\left(\frac{\pi}{2} - \alpha\right) \times Q\right) + \frac{(de_{ol} + at)}{2} \times \sin\left(\frac{\pi}{2} - \alpha\right) \times Q \quad (7)$$

Eq. (6) and Eq. (7) explain the two new defenders with the motion on the basis of the attacker and protector accordingly.

iii) ***Diversion theft:*** Here, at first, the attacker assists the defender to the place. Eq. (8) derives this process.

$$de_{ne} = de_{ol} \times (1 - \sin\ \alpha) \times Q + \frac{\left(de_{ol} + at \times Q \times \sin\left(\frac{\pi}{2} - \alpha\right)\right)}{2} \times \sin\ \alpha \times Q \quad (8)$$

Eq. (8) concentrates to offer the defender motion by taking its present place and the mean of distance among the weighted number of attacker and the defender.

iv) ***Pretext:*** In this process, the attacker baits several traits that are defender's favor and assists the defender. This process is given in Eq. (9).

$$de_{ne} = \left(de_{ol} \times Q \times in\left(\frac{\pi}{2} - \alpha\right)\right) \times (1 - \sin\alpha \times Q) + \frac{\left(\left(de_{ol} + Q \times \sin\left(\frac{\pi}{2} - \alpha\right)\right) + at\right)}{2} \times \sin\ \alpha \times Q \quad (9)$$

Eq. (9) contains two primary factors. The initial one is a weighted number of present protector's places. The next one is the mean distance between the attacker and the weighted defender.

v) ***Respond to attack:*** The upcoming place of the protector is estimated and contrasted with the previous place of the protector. Further, the better place is selected for the protector and if the protector's new place is better than the attacker's is, the attacker and protector are interchanged.

vi) ***Generate the new member as a defender:*** In this, the attacker is annihilated by the protector and generates a new member arbitrarily to do the conditions of SE.

vii) ***Stopping condition:*** The stop criteria can be the highest period of the simulation, like other algorithms or the best outcome's quality ever discovered or other chosen condition by the executor.

viii) The pseudo-code of implemented FPUSA is provided in Algorithm 1. The flowchart of the recommended FPUSA is given in Fig.3.

Algorithm 1: Suggested FPUSA
Assign the data for the optimization problem
Consider the maximum iteration $z_{\max}$ and initialize the defender and attacker de *and* at
Validate the fitness function
For $z = 1$ *to* $z_{\max}$
For $m = 1$ *to* M_{pop}
Derive new arbitrary distribution factor Q using Eq. (1)
Perform train and retrain tasks using Eq. (4)

DOI: https://doi.org/10.54216/FPA.190217
Received: January 11, 2025 Revised: February 18, 2025 Accepted: March 06, 2025

```
        Conduct the spot-on attack operations using Eq. (5) to Eq. (9)
        Produce the new candidate as a defender
    End for
    Save the best outcome
End for
Return best outcome
```

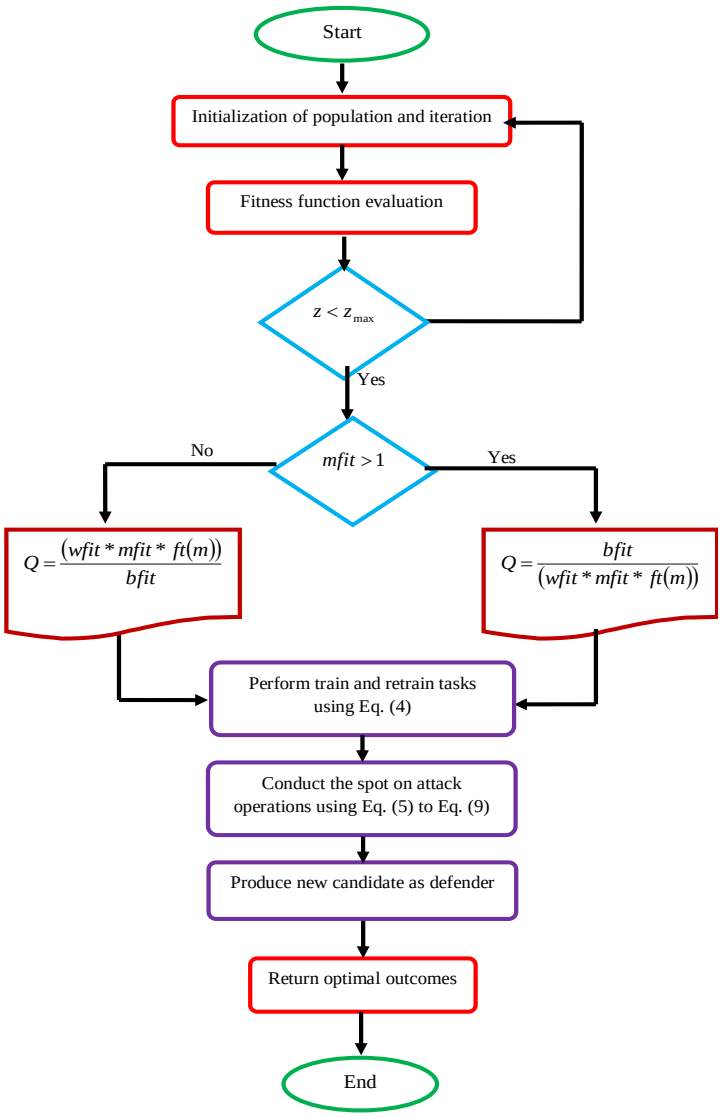

Figure 3. Flowchart of designed FPUSA for optimizing parameters in ALL segmentation and diagonsis processes

4. Abnormality segmentation using Transformer-based ResidualU net+ for ALL Diagonsis

4.1 ResUnet+

The ResUnet+ technique is supported to perform the abnormality segmentation. The Unet technique has a number of disadvantages, despite being used for the segmentation process. The gradient vanishing problem, which arises as the approach becomes deeper, is one of the major drawbacks. As the network gets deeper, the gradient in the lower levels approaches zero.Moreover, when generating the segmentation masks in the Unet technique; the high and low level features that include the data concerning the location, edges, and boundary of the tumor are very

DOI: https://doi.org/10.54216/FPA.190217
Received: January 11, 2025 Revised: February 18, 2025 Accepted: March 06, 2025

significant. In this situation, the significant feature's influence may reduce whereas the unimportant feature's value may enhance. This results in a negative impact on the segmentation process. To mitigate these problems, the ResUnet+ technique is recommended. The ResUnet+ technique is varied from other Unet-aided techniques in that several changes are performed in the technique's encoder state to maintain the low-level attributes and to rectify the vanishing issue. For this purpose, the residual modules are employed. In order to maintain the low-level attributes and rectify the vanishing issues, the residual modules are employed. Because of this, the residual blocks are adopted in the encoder block of the network. Moreover, there are several semantic gaps among the decoder and encoder in the conventional Unet technique. To rectify this issue, unlike the other Unet techniques, new links are inserted among the decoder and encoder. At each node among the decoder-encoder layers, the information at the same level as itself and the lower level values are integrated. In the ResUnet+ technique, the residual blocks include 3x3 and 1x1 convolution tasks. These are inserted into each encoder section to avoid the attributes that are lost as an outcome of the convolutional tasks that are normally employed in the Unet techniques. With this operation, the attributes are improved more prior to the convolution task being employed in every layer. However, these can be still lost features. To avoid this, the nodes are inserted among the decoder and encoder, and these nodes are estimated with the attributes joining from the bottom layer. The features have been forwarded from the lowest layer to the top layer. With the support of the ResUnet+ technique, the vanishing issue, the gap, and attribute loss among the decoder and encoder have been avoided. It enhances the segmentation process highly. The ResUnet+ technique is diagrammatically shown in Fig.4.

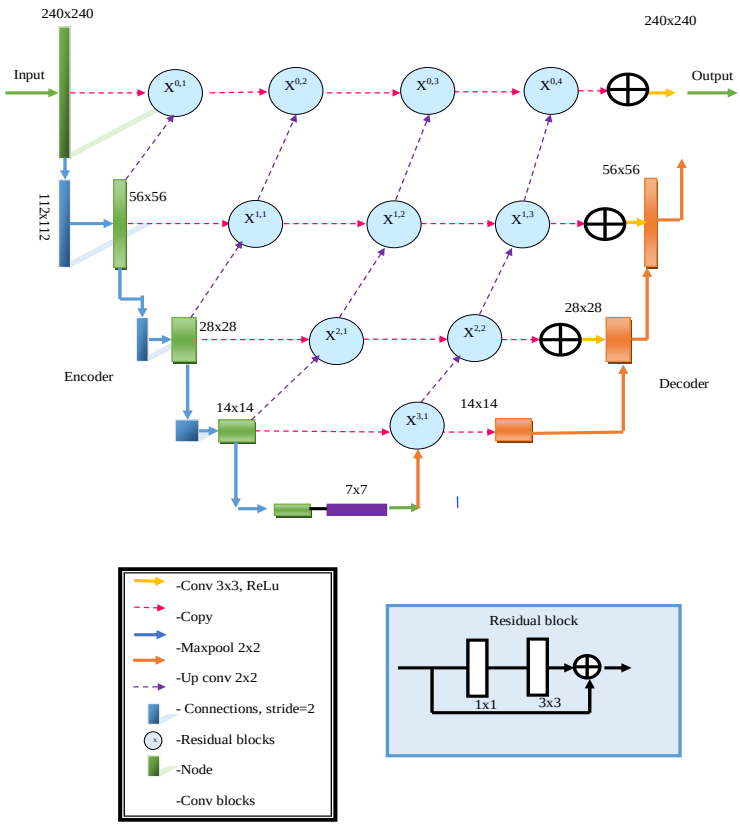

Figure 4. Diagrammatic illustration of ResUnet+ technique for the segmentation process

4.2 Transformer

Utilizing the attention task, the transformer network has been developed, comprising both a decoder and an encoder. There are eight stacked same layers in the transformer with two sub-layers for each layer. The two sub-layers are Multi-Head Attention (MHA) and Fully Connected Forward Neural Network (FCFNN). These two sub-layers are linked with the residual block. After this, the norm layer is attached. Each sub-layer produces the outcome by $op = layernorm(a + sublayer(a))$, where each layer is designed separately.

In order to assist the residual connection among the layers, the technique's sub-layers are limited solutions with 256 dimensions. The network's sub-layers are explained as follows.

DOI: https://doi.org/10.54216/FPA.190217
Received: January 11, 2025 Revised: February 18, 2025 Accepted: March 06, 2025

Scaled dot-product attention: The value va, key ke, and query qu are the inputs for the attention function. The weight of the attention is determined by the query key similarity. The information of the attention is achieved because of attention weights. The technique adopts the scaled dot product attention is determined in Eq. (10).

$$Atn(qu, ke, va) = soft\max\left(\frac{qu * ke_T}{\sqrt{d_{ke} va}}\right) \quad (10)$$

MHA: It projects the va, ke, and qu with the support of diverse sequential transformations and finally connects numerous attention solutions. The va, ke, and qu have the same values in the self-attention process. The derivation is given in Eq. (11) and Eq. (12).

$$MtHead(qu, ke, va) = concat(head_1, \ldots, head_k) \quad (11)$$

$$head_h = Atn\left(qu * w_h^{qu}, ke * w_h^{ke}, va * w_h^{va}\right) \quad (12)$$

Here, the variable $MtHead(qu, ke, va)$ is the $head_i$ contact.

Position-wise Feed-Forward Network (FFN): Encoder's each layer includes FCFFN and two-layer linear transformation, with the attention sub-layer employing the Rectified Linear Unit (ReLU) activation function.

$$FFN(a) = \max(0, aw_1 + x_1)w_2 + x_2 \quad (13)$$

The linear transformations employ diverse attributes from layer to layer since these are same across the distinct places.

Positional encoding: To employ the linear order, the positional encoding is inserted into the input embedding at the upper of the encoder. The dimension of the positional encoding pe is the same as the input embedding.

$$pe_{(pos,2h)} = \sin\left(\frac{pos}{10000^{\frac{2h}{d_{model}}}}\right) \quad (14)$$

$$pe_{(pos,2h+1)} = \sin\left(\frac{pos}{10000^{\frac{2h}{d_{model}}}}\right) \quad (15)$$

Here, the position is denoted as pos, and the dimension is specified as h.

4.3 Proposed OTRUnet+ for Segmentation

The OTRUnet+ is the powerful technique adopted for abnormality segmentation. Here, the gathered input images A_l are fed as input. OTRUnet+ technique is incorporated with the existing transformer and ResUnet+ techniques. The transformer technique mitigates the issues of scattered target regions and huge shape variations in the segmentation operations because of its merits of attaining global context. The ResUnet+ approach employs very low parameters and offers better performance. However, the ResUnet+ technique may generate low-quality images while processing large amounts of images. This minimizes the efficiency and accuracy of the ALL diagnosis process. Therefore, the transformer network is integrated into the ResUnet+ approach in order to enrich the quality of the segmented images. This positively influences the ALL diagnosis process. Thus, the TRUnet+ technique is developed. This technique not only enhances the quality of the images but also increases the efficacy. Even though the recommended TRUnet+ technique produces high-quality segmented images, the parameters of this approach such as epochs, steps per epoch, and hidden neurons get increased that leads to data overhead and overfitting complexities. Therefore, optimizing the mentioned parameters offers a significant part in reducing the issues in the segmentation process. In order to optimize the TRUnet+ technique parameters the FPUSA approach is suggested. This algorithm has higher convergence rates and quickly selects the optimal solutions. Hence, the OTRUnet+ technique is presented for the segmentation operation with the assistance of the recommended FPUSA approach. The objective function of the operation is offered in Eq. (16).

$$ob_1 = \underset{\{hn^{TRUnet+}, ep^{TRUnet+}, se^{TRUnet+}\}}{\arg\max}\left[dc + ac\right] \quad (16)$$

DOI: https://doi.org/10.54216/FPA.190217
Received: January 11, 2025 Revised: February 18, 2025 Accepted: March 06, 2025

Here, the hidden neuron count of TRUnet+ is indicated as $hn^{TRUnet+}$ with the boundary of [5, 255]. The amount of epochs in TRUnet+ is specified as $ep^{TRUnet+}$ with the limit of [5, 50]. The steps per epoch in TRUnet+ are specified as $se^{TRUnet+}$ with the limit of [300, 1000]. The accuracy ac and dice coefficient dc values are maximized by this process. These attributes are given as follows.

Accuracy ac *:* An attribute defines how effectively the approach works in the overall process. Eq. (17) offers its mathematical formulation.

$$Ac = \frac{ss + fs}{ss + fs + hh + kk} \tag{17}$$

Dice coefficient dc *:* It is the statistical measure utilized to gauge the similarity of the two samples. Eq. (18) gives its mathematical formulation.

$$Dc\left(A_l, A_l^{seg}\right) = \frac{2\left(A_l \cap A_l^{seg}\right)}{\left(A_l + A_l^{seg}\right)} \tag{18}$$

In this, the "true negative and true positive" values are denoted as ff *and* kk. The "false negative and false positive" values are declared as ss *and* hh.

In the end, the high potential network named OTRUnet+ obtains the segmented images and the received segmented images are specified as A_l^{seg}. The designed OTRUnet+ strategy's structure is provided in Fig.5.

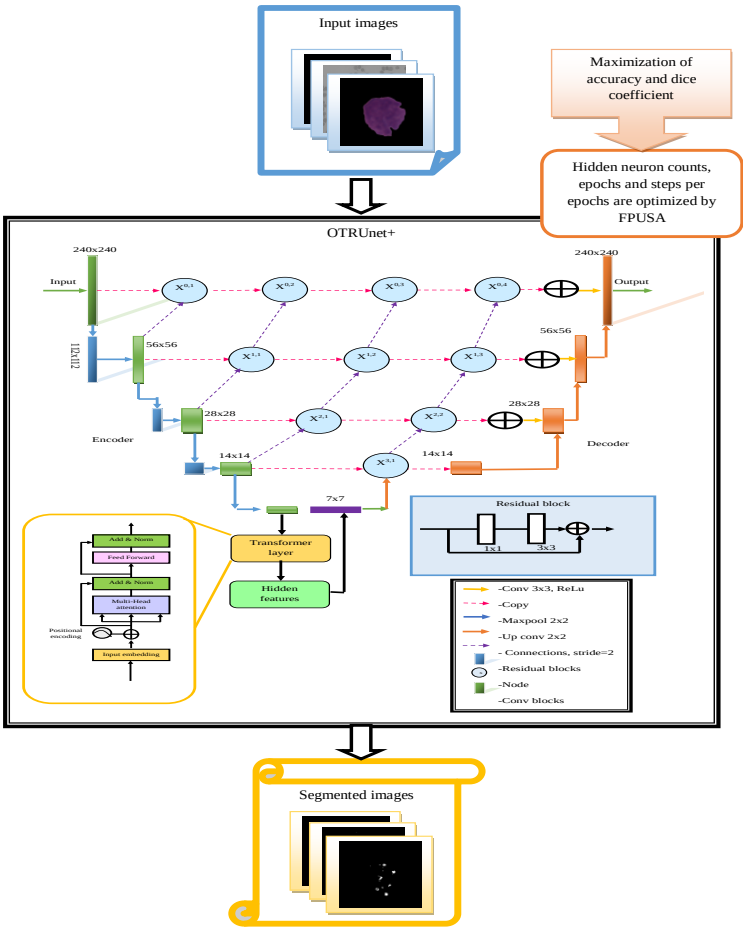

Figure 5. Structure of recommended OTRUnet+ technique for abnormality segmentation

DOI: https://doi.org/10.54216/FPA.190217
Received: January 11, 2025 Revised: February 18, 2025 Accepted: March 06, 2025

5. Adaptive Multi-dilated RAN for ALL Disease Detection with its Objective function

5.1 Residual Attention Network

By stacking diverse attention blocks, the RAN is constructed. Here, each attention block is categorized into two branches called "trunk branch and mask branch". The trunk branch that is resilient for modern network models conducts the processing. Consider the input as d and the solution of the trunk branch is given as $Tr(d)$. The similar size $Tr(d)$ employed by the mask branch mask Ma as the "bottom-up and top-down" framework. This simplifies the resultant feature $Tr\ weight\ learn(d)$. The "bottom-up and top-down" copy the feedback and feed-forward attention task. For the stem-branching neurons, the resultant mask is employed as the control gate in the highway network. The attention block's result A is given using Eq. (19).

$$A_{k,s}(d) = Q_{k,s}(d) + Tr_{k,s}(d) \tag{19}$$

Here, the variable k extends the overall spatial region and the variable $s \in \{1,...,S\}$ defines the channel index. In the attention block, the attention mask performs as the function selector in the forward interference and gradient update filter in the backpropagation. The given feature mask's gradient is derived in Eq. ().

$$\frac{\partial Ma(d,\theta)Tr(d,\phi)}{\partial \phi} = Ma(d,0)\frac{\partial Tr(d,\phi)}{\partial \phi} \tag{20}$$

Here, the parameters of the trunk and mask branch are given as $\phi\ and\ \theta$ respectively. This feature makes the attention block effective over noisy labels. The mask branches avoid the false gradients and trunk attributes are upgraded.

5.2 Suggestive Disease Classification System: AMDRAN

The AMDRAN technique is introduced for performing the ALL diagnosis in this work. This technique employed the segmented images A_l^{seg} as input. Basically, the AMDRAN technique is composed of a multi-dilated mechanism and the RAN technique. The RAN technique is robust to noise labels and grasps the rich features of the segmented images. However, the RAN technique troubles the gradient issues. To eliminate this problem, the multi-dilated convolution is integrated into this technique. The multi-dilated convolution [30] has the ability to alleviate the gradient issues and also mitigate the aliasing issues. Moreover, the multi-dilated convolution combines the information from local to wide data of a highly huge receptive field in a separate layer. The multi-dilated convolution is expressed in Eq. (21).

$$W_g \otimes_g^s q_g = \sum_{f=0}^{g-1} w_f \otimes_{a_f}, z_g^f \tag{21}$$

Here, the variable $W_g = \lfloor w_0,...w_{g-1} \rfloor = \psi(\lfloor b_0,...,b_g - 1 \rfloor)$ indicates the solution of the composite layer, and the multi-dilated convolution is given as $\otimes_g^s$. The dilation factor is indicated as a_f and the filter subset related to the fth skip connection is given as z_g^f. Thus, the multi-dilated convolution is integrated with the RAN technique and generates the network named MDRAN. This network minimizes the limitations faced in the RAN technique and highly enhances the classification process. Moreover, it reduces the dimensionality issues. Though this technique produces effective outcomes, it may consume more amount of time to generate the classified outcomes since it has more amounts of parameters such as epochs, activation functions, and hidden neurons. Therefore, optimally determining the network parameters is significant. The designed FPUSA approach is suggested for this purpose. This FPUSA optimally determines the mentioned parameters and reduces the processing time of the network. Thus, the AMDRAN technique is designed for the ALL classification process by employing the FPUSA approach. The objective function of this operation is shown in Eq. (22).

$$ob_2 = \underset{\{hn^{MDRAN}, ep^{MDRAN}, af^{MDRAN}\}}{\arg\max} [ac] \tag{22}$$

Here, the MDRAN approach's hidden neuron count is declared as hn^{MDRAN} with the limit of [5, 255]. The MDRAN network's number of epochs is denoted as ep^{MDRAN} with the limit of [5, 50]. The MDRAN network's activation function is denoted as af^{MDRAN} with the limit of [1, 5]. The accuracy ac also maximized in this process and the

DOI: https://doi.org/10.54216/FPA.190217
Received: January 11, 2025 Revised: February 18, 2025 Accepted: March 06, 2025

accuracy ac is measured in Eq. (17). Thus, the AMDRAN technique produces ALL classified outcomes effectively in terms of benign and malignant. The AMDRAN-based ALL classification process is diagrammatically depicted in Fig.6.

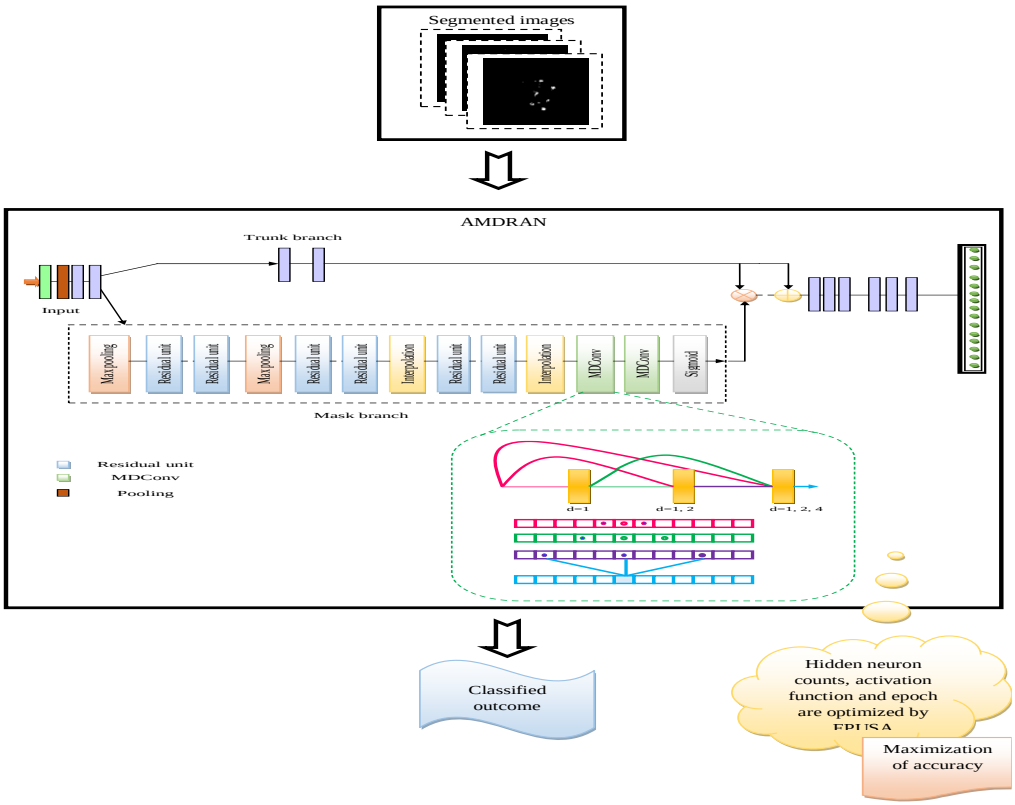

Figure 6. Diagrammatic representation of AMDRAN-based ALL classification

5.3 Resultant Images

The presented OTRUNet+-based segmentation operation helps to segment abnormalities that exist in the provided images and produces high-quality segmented images. The resultant images are shown in Fig.7 contrasted with conventional segmentation techniques.

"Images"	**1**	**2**	**3**	**4**	**5**
"Dataset 1"					
"Original"					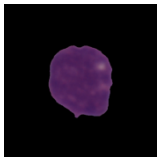
"Ground truth"	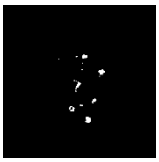				

DOI: https://doi.org/10.54216/FPA.190217
Received: January 11, 2025 Revised: February 18, 2025 Accepted: March 06, 2025

"Unet [23]"					
"Unet3+ [24]"					
"TransUnet [25]"		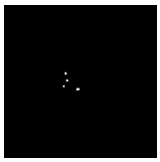			
"TRUnet [26]"		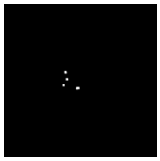			
Suggested OTRUnet+	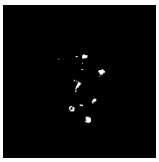				
"Dataset 2"					
"Original"	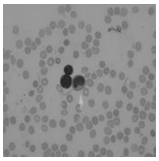	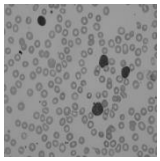	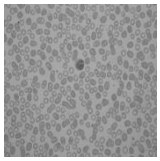	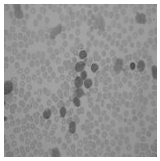	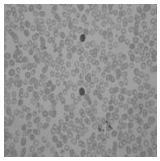
"Ground truth"	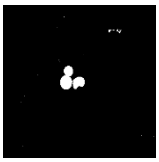	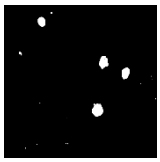	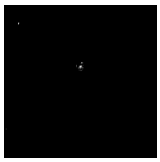	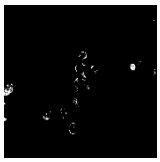	
"Unet [23]"	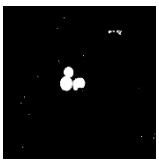	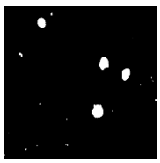	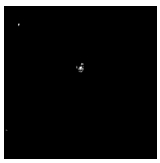	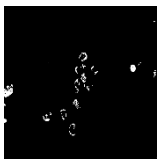	
"Unet3+ [24]"	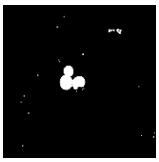	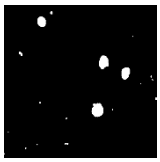	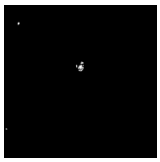	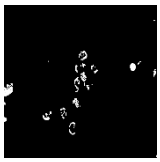	

DOI: https://doi.org/10.54216/FPA.190217
Received: January 11, 2025 Revised: February 18, 2025 Accepted: March 06, 2025

"TransUnet [25]"		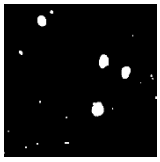	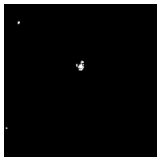	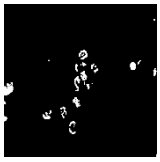	
"TRUnet [26]			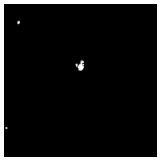	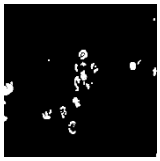	
Suggested OTRUnet+	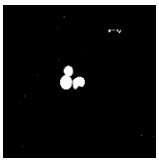	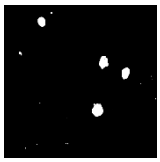	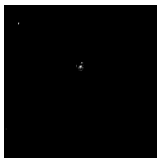	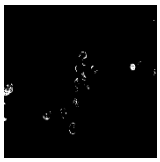	

Figure 7. Resultant images of OTRUnet3+-based abnormality segmentation process over traditional segmentation techniques

6. Results and Discussions

6.1 Simulation Setup

The designed ALL diagnosis mechanism was implemented by the Python platform and significant outcomes were achieved. The recommended FPUSA approach employed 50 iterations as a maximum, 10 populations, and 3 chromosome lengths. In order to verify the performance of the designed ALL classification process, the traditional algorithms such as "Tomtit Flock Metaheuristic Optimization Algorithm (TFMOA) [18], Cicada Swarm Optimization (CSO) [19], Zebra Optimization Algorithm (ZOA) [20], and SEO [16]" were taken. Also, some of the existing classifiers such as "CNN [21], Densenet [22], RAN [17], and MDRAN [17] [23]" were taken. Some of the conventional segmentation techniques such as "Unet [23], Unet3+ [24], TransUnet [25], and TRUnet+ [26] were taken.

6.2 Performance metrics

The necessary performance factors employed in the ALL classification process are given as follows.

Accuracy: It is calculated in Eq. (17).

Dice coefficient: It is estimated in Eq. (18).

Jaccard: It is calculated in Eq. (23).

$$jc\left(A_l, A_l^{seg}\right) = \frac{\left(A_l \cap A_l^{seg}\right)}{\left(A_l \cup A_l^{seg}\right)} \tag{23}$$

FDR: It is estimated in Eq. (24).

$$FDR = \frac{hh}{ss + hh} \tag{24}$$

FNR: It is calculated in Eq. (25).

$$FNR = \frac{kk}{ss + kk} \tag{25}$$

FPR: It is calculated in Eq. (26).

$$FPR = \frac{hh}{hh + ss} \tag{26}$$

NPV: It is calculated in Eq. (27).

DOI: https://doi.org/10.54216/FPA.190217
Received: January 11, 2025 Revised: February 18, 2025 Accepted: March 06, 2025

$$NPV = \frac{ss}{ss + kk} \quad (27)$$

Precision: It is estimated in Eq. (28).

$$P = \frac{ss}{ss + hh} \quad (28)$$

6.3 Confusion matrix analysis of recommended ALL classification process

The recommended ALL classification process is evaluated with the confusion matrix for two data sources and it is shown in Fig.8. Based on the original and predicted values, the accuracy of the process is estimated. The confusion matrix depicts how the predictions are conducted by the classification technique that is confused and disorganized. From Fig.8 (b), it has been ensured that, while processing the images of second dataset, a higher accuracy (97.33%) is achieved than the first dataset. Thus, it has been confirmed that the presented ALL classification process offers high-accuracy outcomes for both datasets.

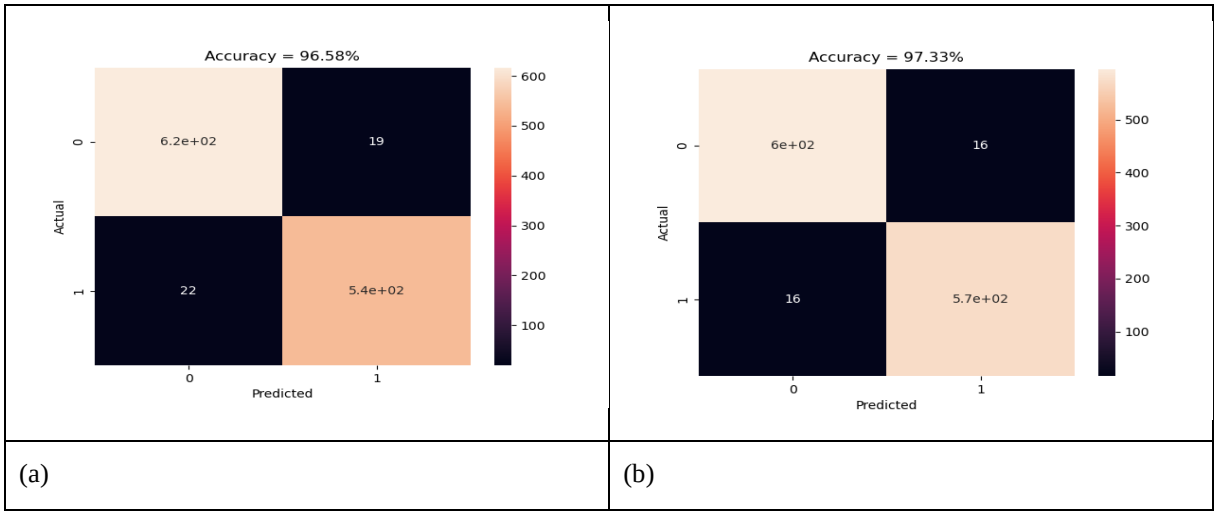

(a) (b)

Figure 8. Confusion matrix evaluation of suggested ALL classification process in terms of " (a) Dataset 1, and (b) Dataset 2"

6.4 Convergence analysis of the FPUSA algorithm

Fig.9 offers the convergence estimation of the presented FPUSA task over existing algorithms. The convergence analysis helps to find out the recommended FPUSA approach's performance over traditional algorithms. Here, the iteration values are helped to evaluate the convergence of the presented FPUSA. When considering the 35th iteration in Fig.9

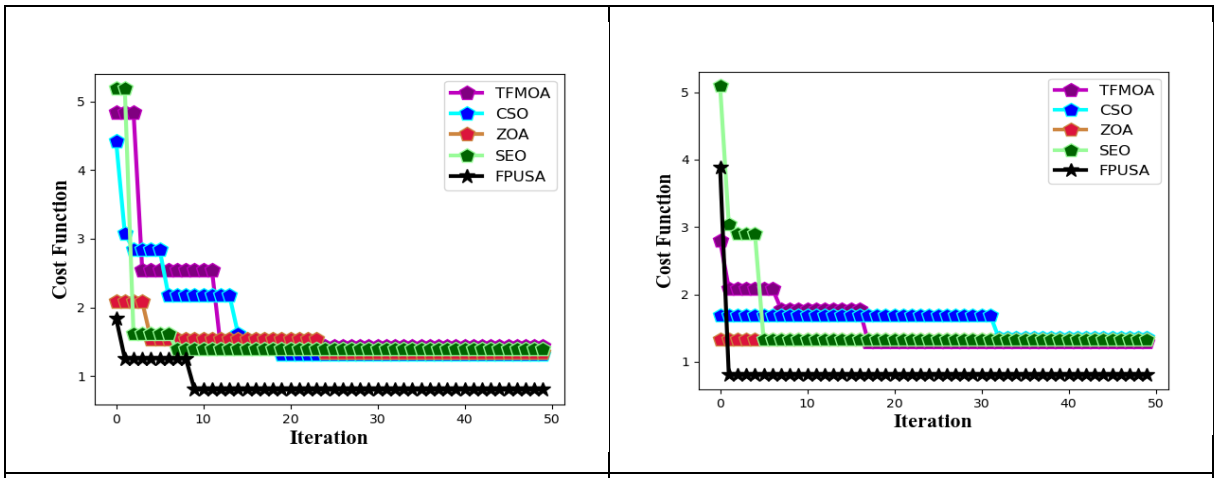

(a) (b)

DOI: https://doi.org/10.54216/FPA.190217
Received: January 11, 2025 Revised: February 18, 2025 Accepted: March 06, 2025

Figure 9. Convergence estimation of suggested FPUSA task over traditional algorithms in terms of "

(a) Dataset 1, and (b) Dataset 2"

(a), the implemented FPUSA approach's convergence is developed by 75% of TFMOA, 65% of CSO, 72.5% of ZOA, and 72.5% of SEO correspondingly. Thus, it has been confirmed that the recommended FPUSA achieved higher convergence rates than the traditional algorithms. Moreover, it has been ensured that the presented FPUSA can recognize the possible optimal solutions more quickly than the conventional algorithms.

6.5 Statistical analysis of the FPUSA algorithm

The statistical evaluation of the FPUSA approach is presented in Table II over conventional algorithms by employing statistical measures. The best factor specifies the alpha value, whereas the worst value specifies the function value at the worst outcome. The mean factor illustrates the average of the best value on the other hand the median factor illustrates the alpha score's median value. The standard deviation (std) estimates how close the data source is to the mean. Thus, these factors are taken for evaluating the FPUSA algorithm. When considering the best metric in a second data source, the performance of the FPUSA is enhanced by 61.25% of TFMOA, 68.75% of CSO, 66.25% of ZOA, and 65% of SEO respectively. Thus, it has been confirmed that the presented FPUSA approach attained promising functionality rates than the traditional algorithms.

Table 2: Statistical Evaluation of Recommended FPUSA Algorithm over Existing Algorithms

Terms	TFMOA [18]	CSO [19]	ZOA [20]	SEO [16]	FPUSA
"Dataset 1"					
"Best"	1.429294323	1.314323347	1.341943362	1.39577245	0.801071184
"Worst"	4.844491863	4.424774035	2.080038404	5.186955451	1.842860716
"Mean"	1.835342975	1.688953373	1.478830573	1.569094065	0.894688524
"Median"	1.429294323	1.314323347	1.341943362	1.39577245	0.801071184
"Std"	0.871604594	0.652420048	0.199980364	0.741336705	0.214591505
"Dataset 2"					
"Best"	1.29744308	1.350103089	1.330621134	1.323897835	0.801395156
"Worst"	2.797260652	1.688735336	1.330621134	5.090953334	3.886762299
"Mean"	1.518858403	1.566827727	1.330621134	1.527868553	0.863102499
"Median"	1.29744308	1.688735336	1.330621134	1.323897835	0.801395156
"Std"	0.342952619	0.162543479	0	0.670308635	0.4319514

6.6 ROC analysis of suggested ALL classification process

The ROC of the suggested ALL classification process is validated by fluctuating the FPR values and given in Fig.10. This analysis contrasted the suggested FPUSA-AMDRAN with traditional classifiers to guarantee the effectualness of the ALL system. The ROC is supported to determine the functionality of the classification process. When considering the FPR value as 0.8 in Fig.10 (b), the presented FPUSA-AMDRAN-based classification operation enriched by 5.26% of CNN, 8.42% of Densenet, 9.47% of RAN, and 4.21% of MDRAN respectively.

DOI: https://doi.org/10.54216/FPA.190217
Received: January 11, 2025 Revised: February 18, 2025 Accepted: March 06, 2025

Hence, it has been proved that the suggested ALL classification approach attained promising efficacy than the existing classifiers.

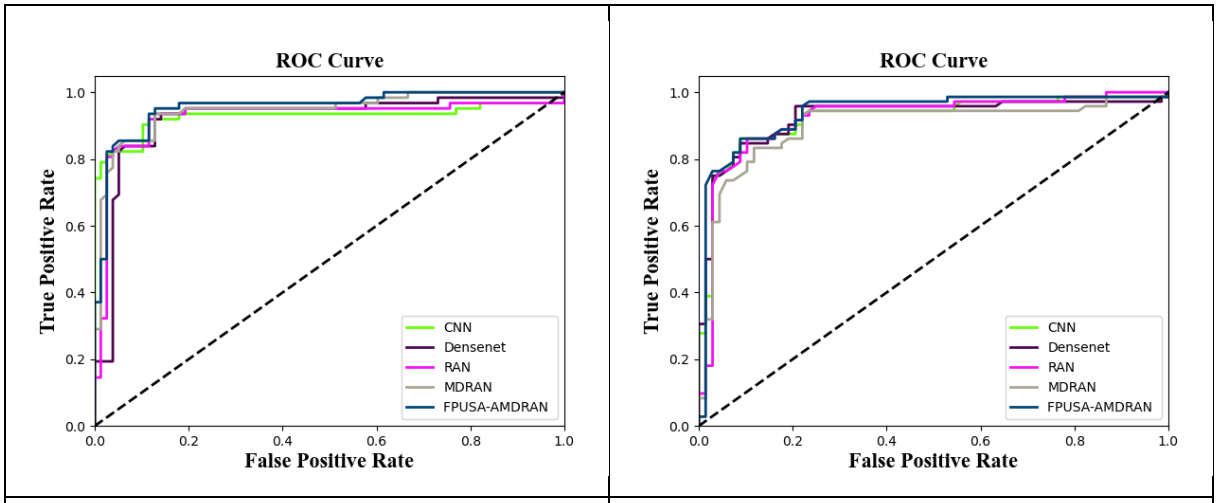

(a) (b)

Figure 10. ROC analysis of presented ALL classification process over existing classifiers in terms of " (a) Dataset 1, and (b) Dataset 2"

6.7 Performance analysis of the segmentation process for dataset 1 and dataset 2

The performance analysis of the segmentation process is carried out by employing statistical measures. Fig.11 and Fig.12 elucidate the performance evaluation of the segmentation process for first dataset over existing algorithms and segmentation techniques. Fig.13 and Fig.14 show the performance evaluation of the segmentation process for second dataset over existing algorithms and techniques. The measures accuracy, Jaccard, and dice coefficient are supported to perform this task. When focussing on the mean metric in Fig.11 (a), the FPUSA-OTRUnet+-based segmentation process achieves 7.77%, 5.55%, 4.44%, and 3.33% higher accuracy than the conventional algorithms TFMOA-OTRUnet+, CSO-OTRUnet+, ZOA-OTRUnet+, and SEO-OTRUnet+ respectively. For the second data source also, the recommended segmentation process offers improved functionality rates. This elucidates the efficacy of the presented segmentation process over traditional approaches.

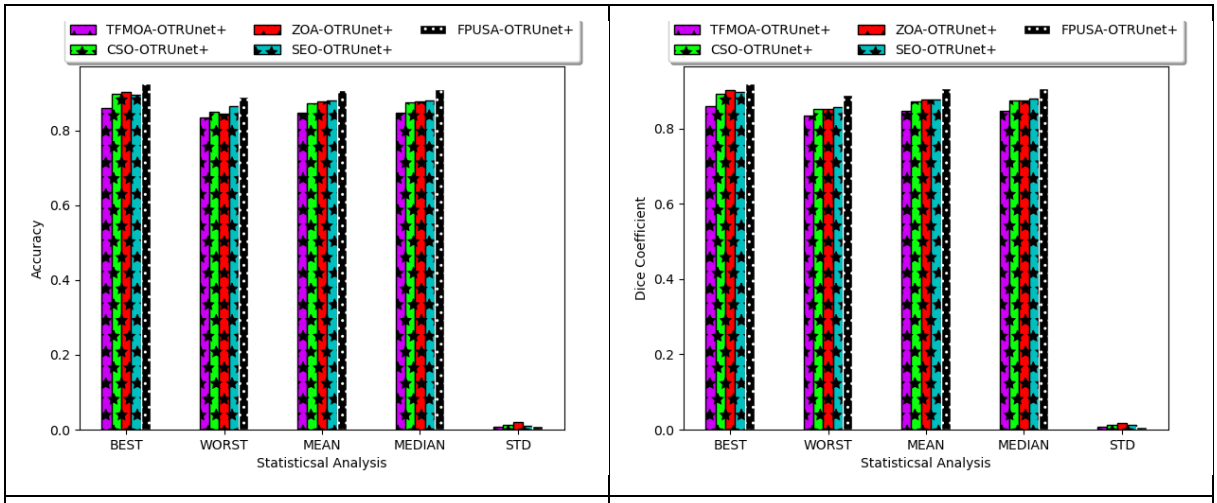

(a) (b)

DOI: https://doi.org/10.54216/FPA.190217
Received: January 11, 2025 Revised: February 18, 2025 Accepted: March 06, 2025

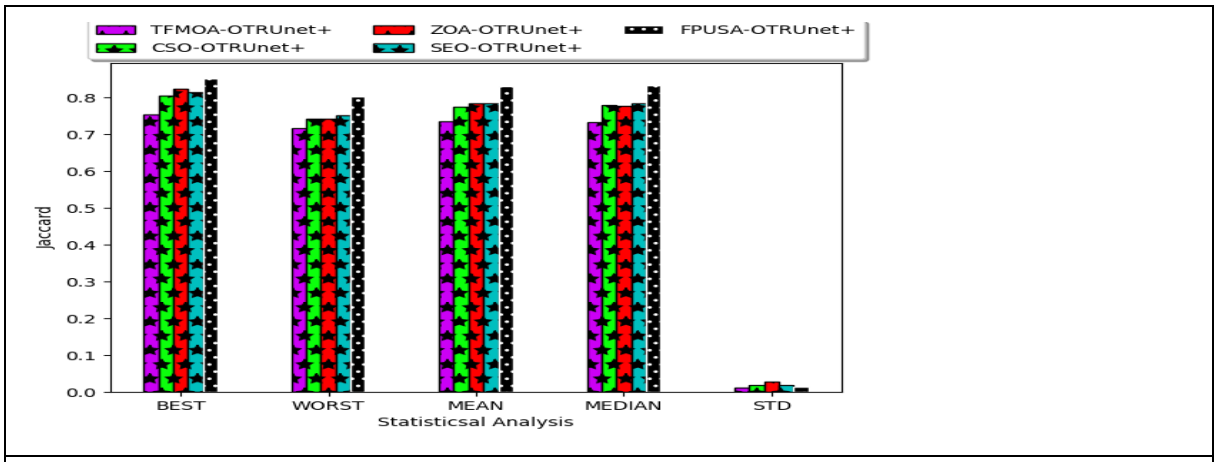

(c)

Figure 11. Performance evaluation of suggested segmentation process for dataset 1 over traditional algorithms concerning " (a) Accuracy, (b) Dice coefficient, and (c) Jaccard"

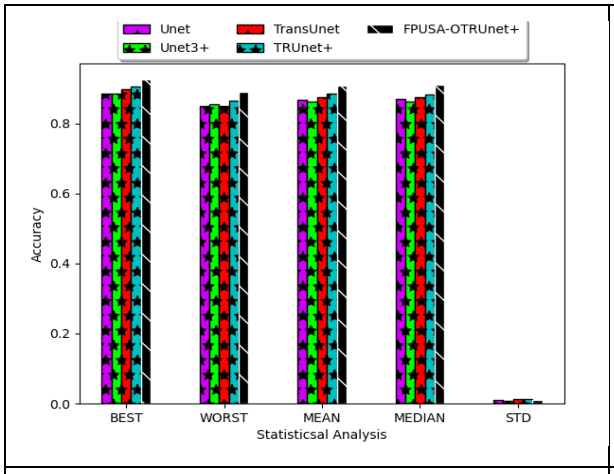

(a)

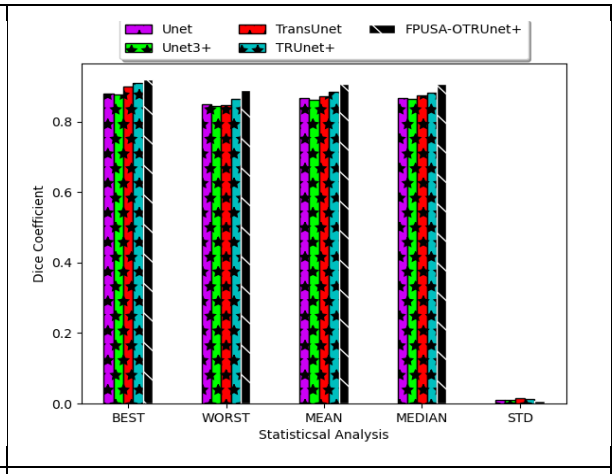

(b)

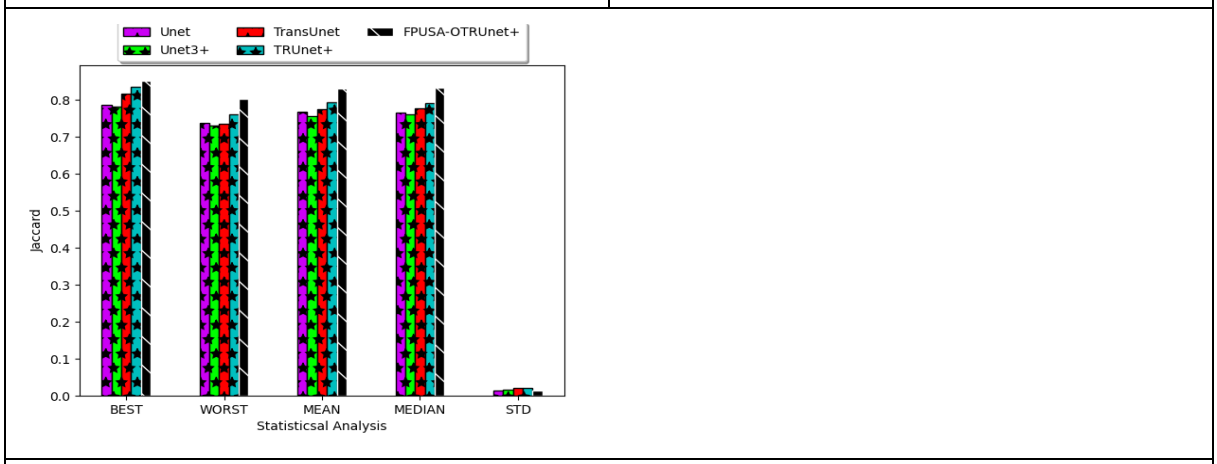

(c)

Figure 12. Performance analysis of suggested segmentation process for dataset 1 over traditional segmentation techniques concerning "(a) Accuracy, (b) Dice coefficient, and (c) Jaccard"

DOI: https://doi.org/10.54216/FPA.190217
Received: January 11, 2025 Revised: February 18, 2025 Accepted: March 06, 2025

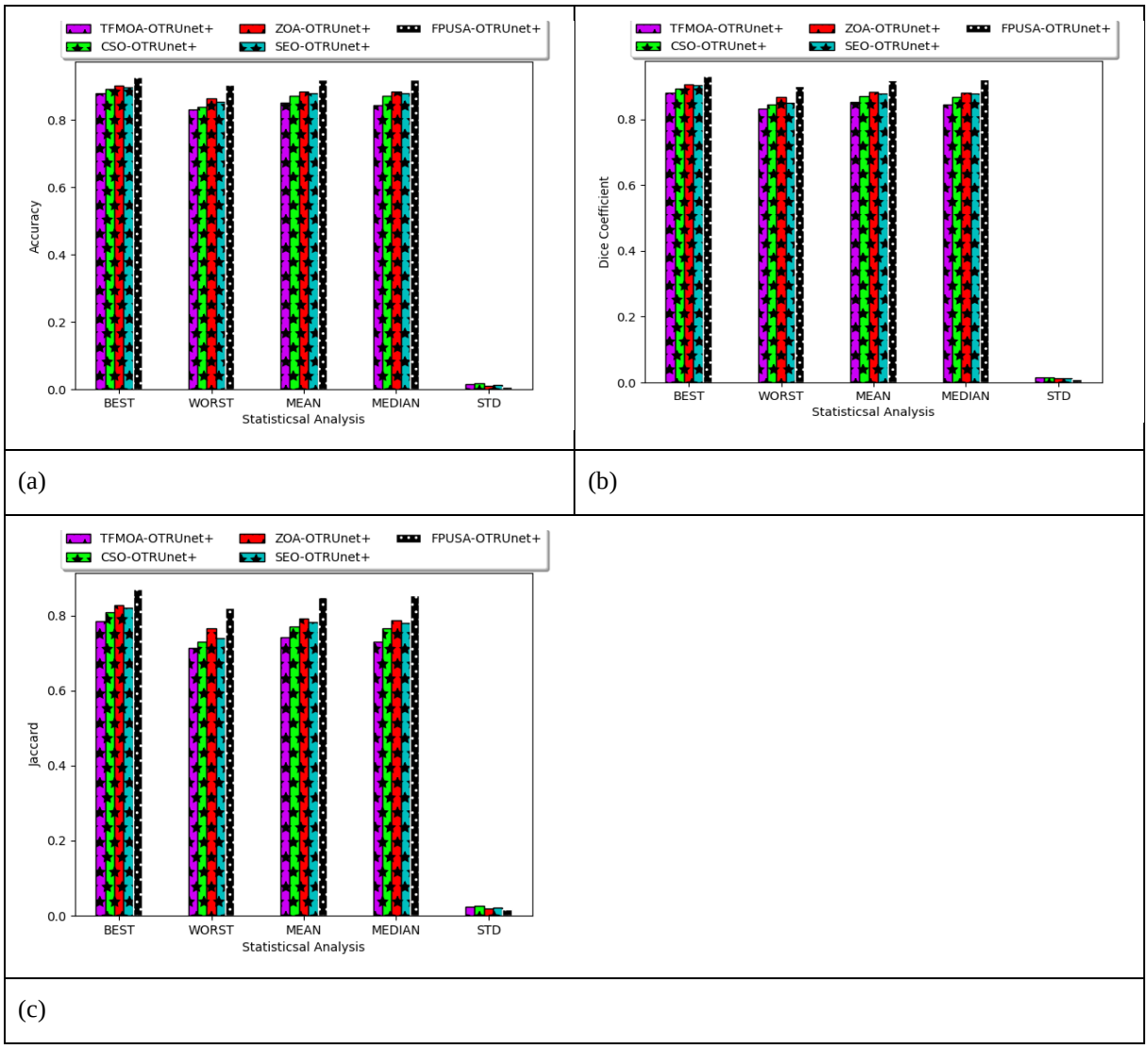

Figure 13. Performance analysis of suggested segmentation process for dataset 2 over traditional algorithms concerning " (a) Accuracy, (b) Dice coefficient, and (c) Jaccard"

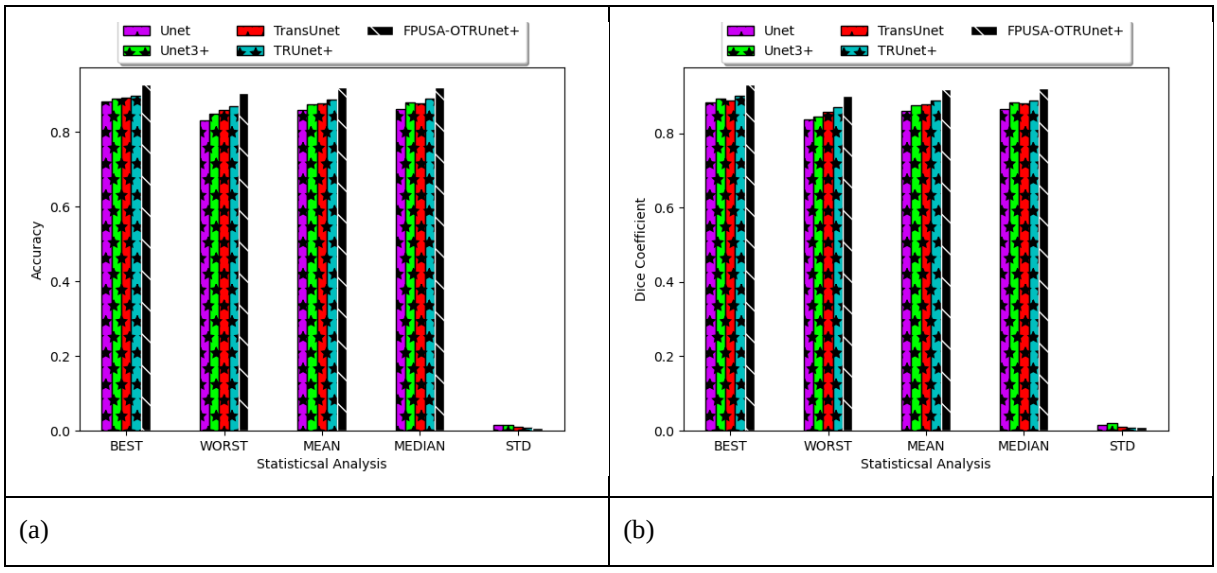

DOI: https://doi.org/10.54216/FPA.190217
Received: January 11, 2025 Revised: February 18, 2025 Accepted: March 06, 2025

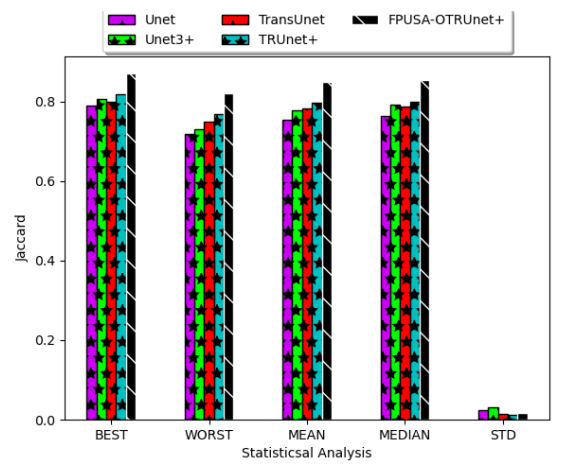

(c)

Figure 14. Performance analysis of suggested segmentation process for dataset 2 over traditional segmentation techniques concerning " (a) Accuracy, (b) Dice coefficient, and (c) Jaccard"

6.8 Performance analysis of ALL classification process for dataset 1 and dataset 2

The presented ALL classification approach's performance is validated for two datasets by employing the batch size values. Fig.15 and Fig.16 depict the performance analysis of ALL classification for dataset 1 over algorithms and techniques. Fig.17 and Fig.18 depict the functionality analysis of ALL classification for dataset 2 over algorithms and techniques. The batch size-based analysis helps to display the generalization capabilities of the recommended ALL process. From Fig.18 (f), the presented ALL classification mechanism's precision is improved by 12.63% of CNN, 10.52% of Densenet, 11.05% of RAN, and 8.42% of MDRAN accordingly when the value of batch size is 32. Thus, it hasbeen ensured that the presented ALL classification framework attained more promising outcomes than the conventional approaches. Moreover, it has been elaborated that the designed ALL classification process effectively supports the medical experts to treat the patients quickly.

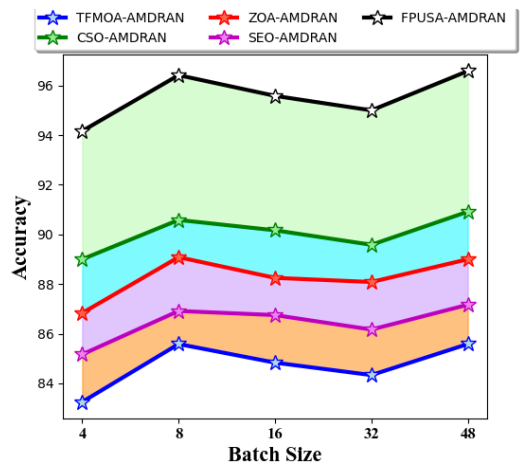

(a)

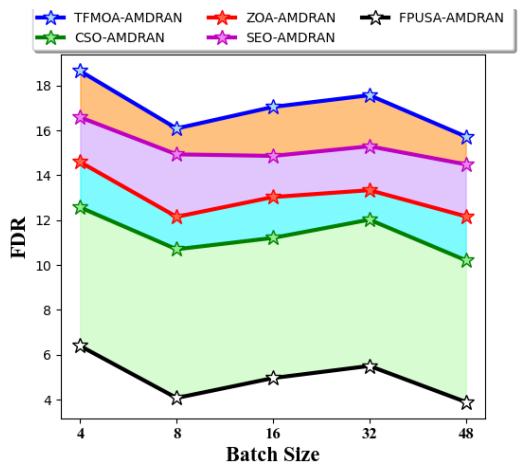

(b)

DOI: https://doi.org/10.54216/FPA.190217
Received: January 11, 2025 Revised: February 18, 2025 Accepted: March 06, 2025

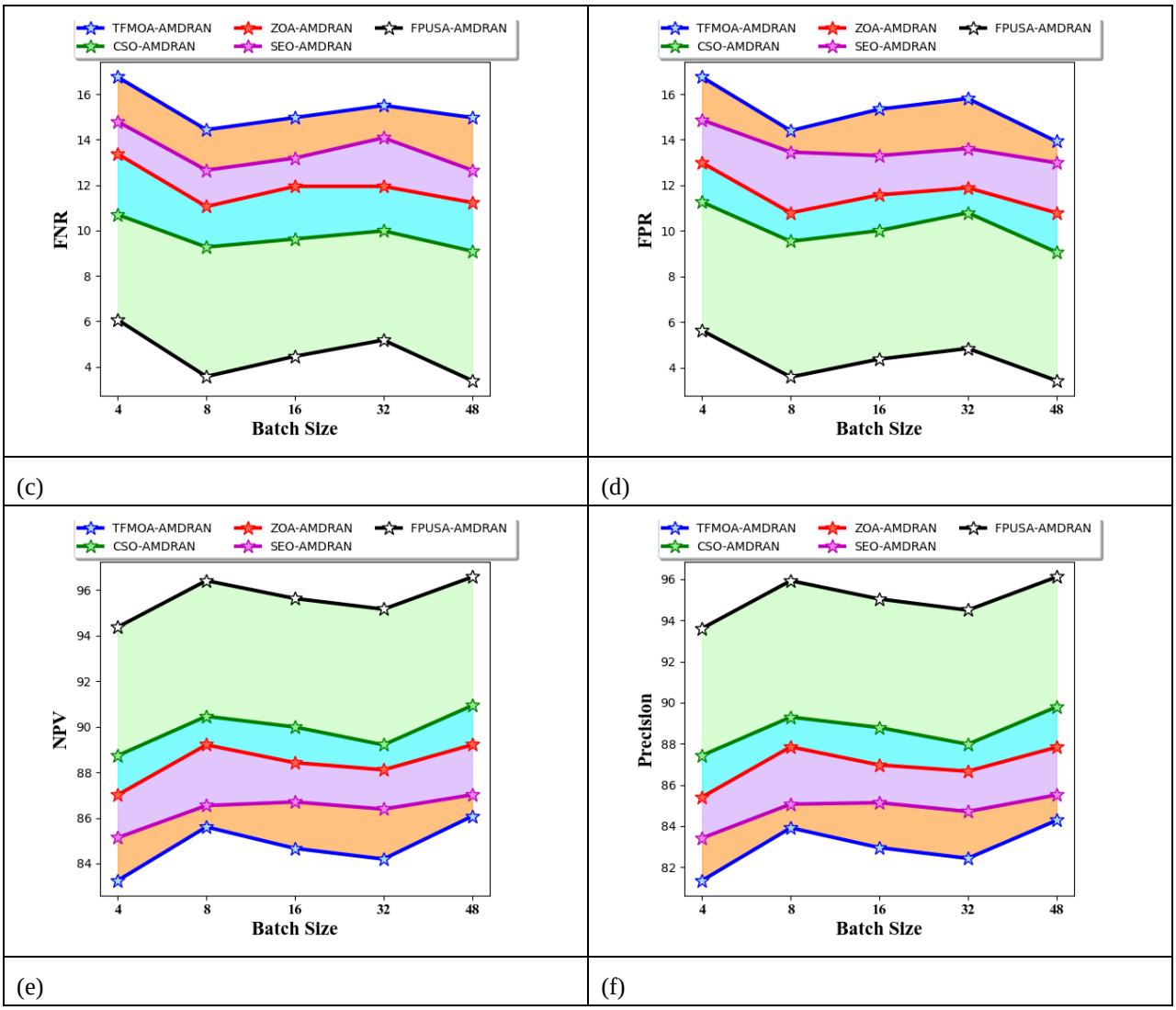

Figure 15. Performance analysis of designed ALL classification framework for dataset 1 over conventional algorithms regarding " (a) Accuracy, (b) FDR, (c) FNR, (d) FPR, (e) NPV, and (f) Precision"

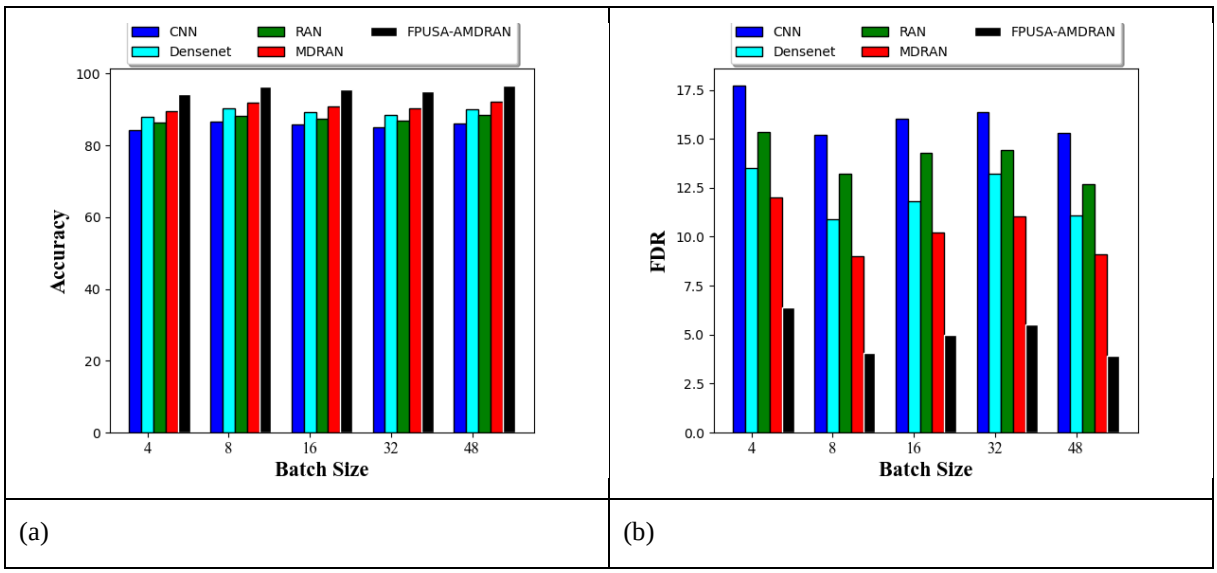

DOI: https://doi.org/10.54216/FPA.190217
Received: January 11, 2025 Revised: February 18, 2025 Accepted: March 06, 2025

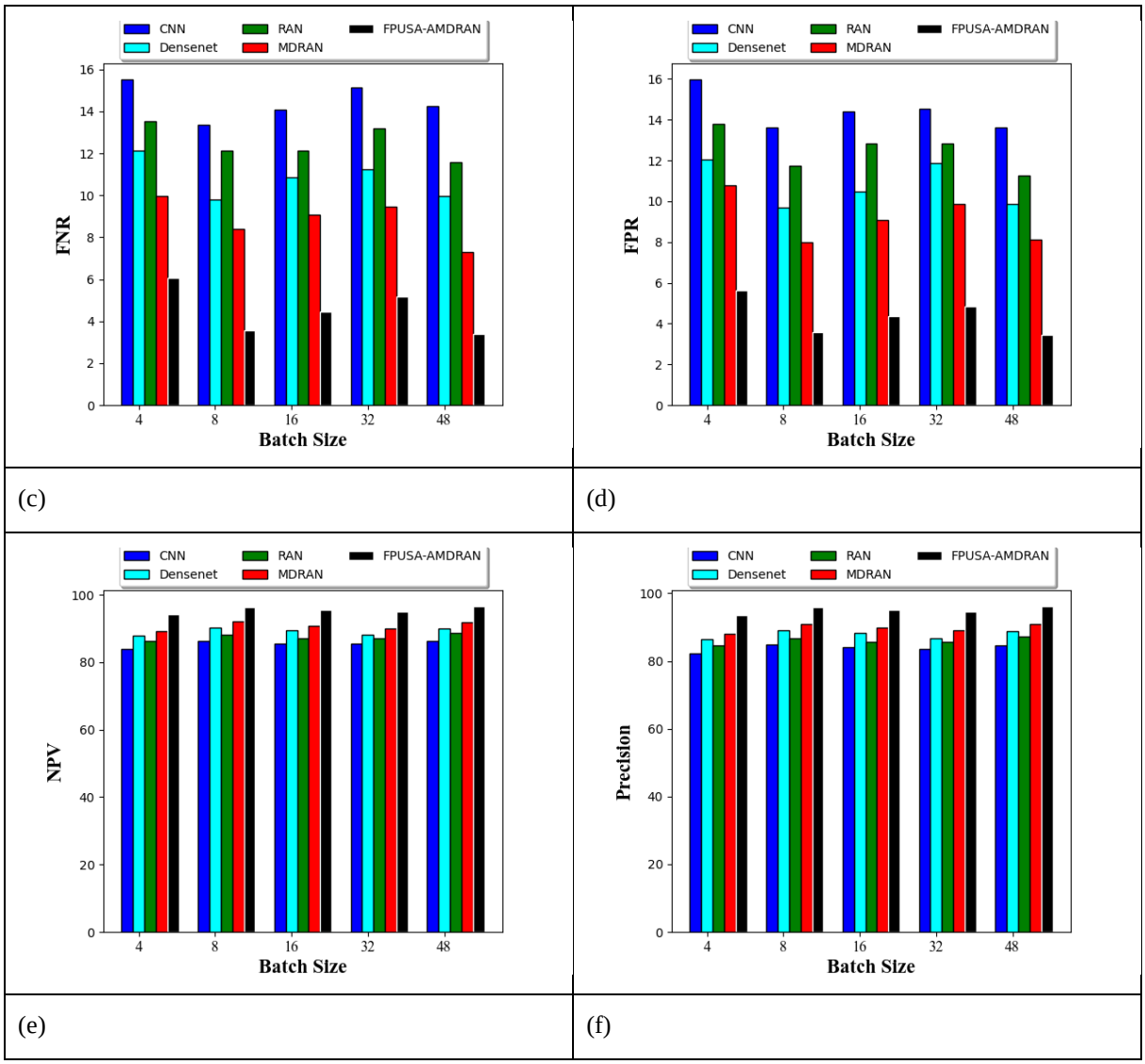

Figure 16. Performance analysis of designed ALL classification framework for dataset 1 over conventional classifiers regarding " (a) Accuracy, (b) FDR, (c) FNR, (d) FPR, (e) NPV, and (f) Precision"

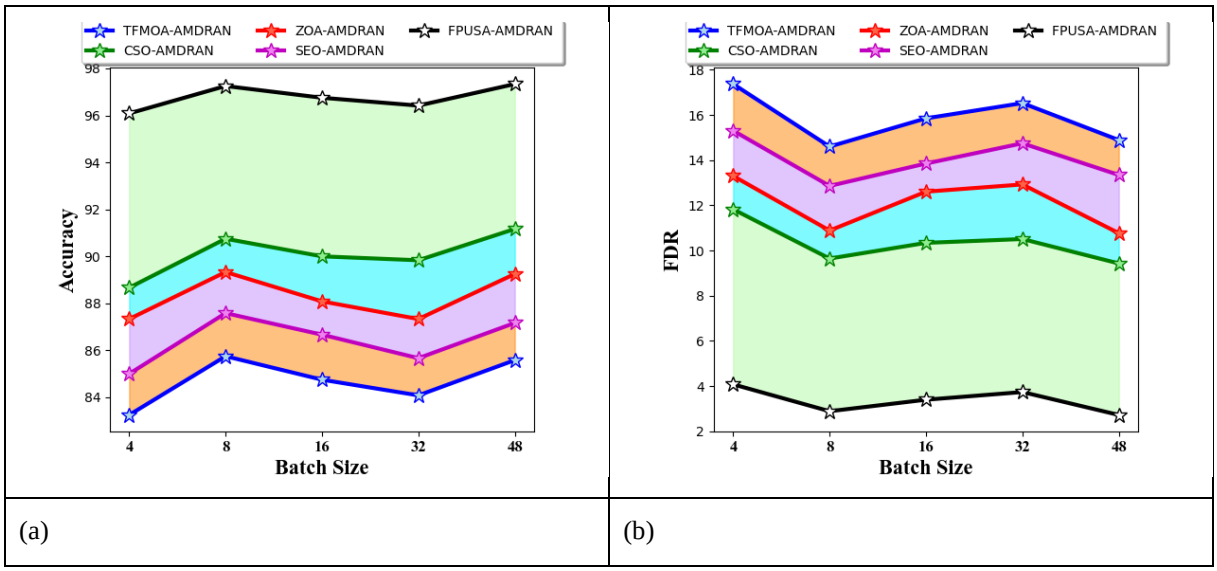

DOI: https://doi.org/10.54216/FPA.190217
Received: January 11, 2025 Revised: February 18, 2025 Accepted: March 06, 2025

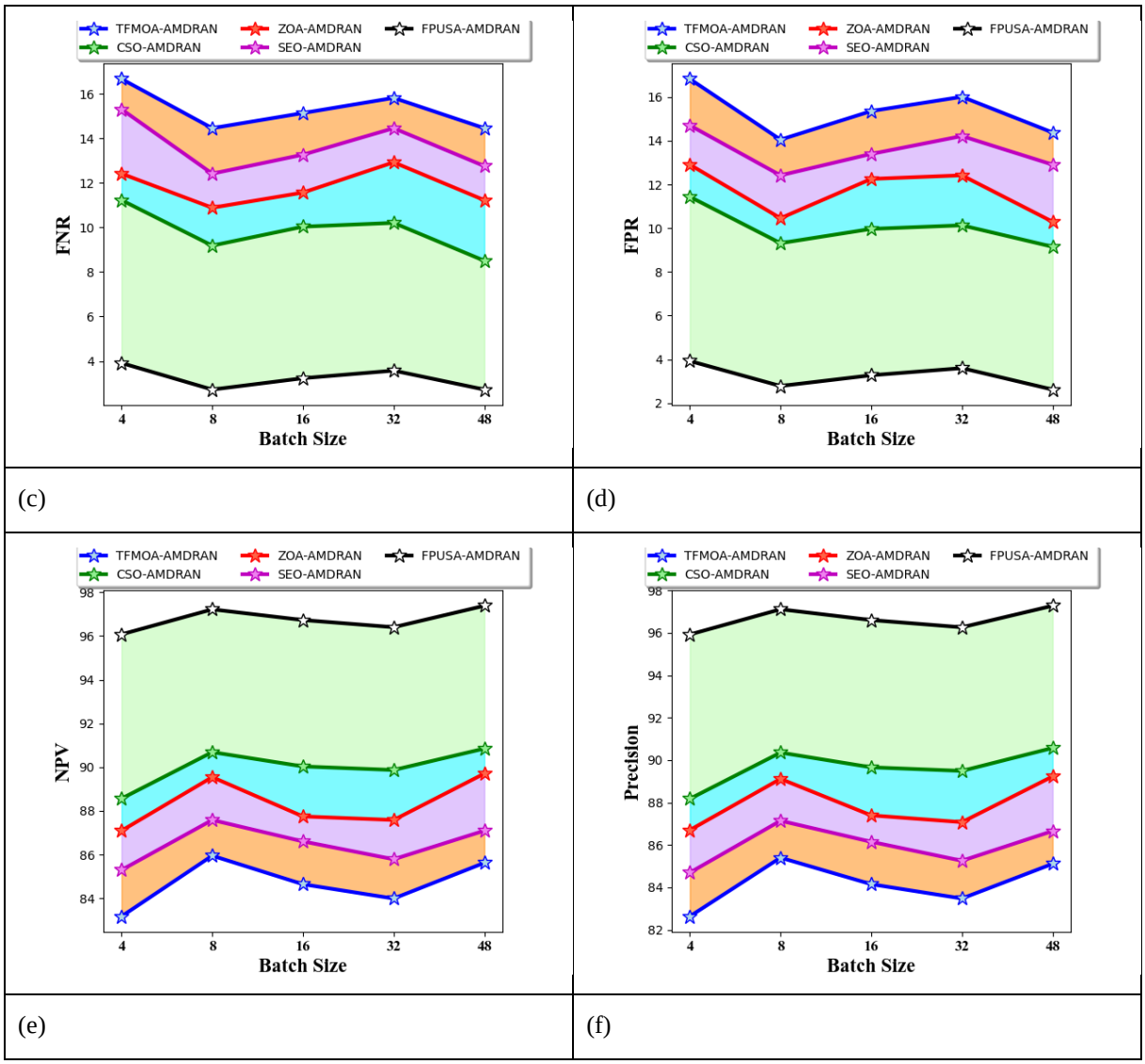

Figure 17. Performance analysis of designed ALL classification framework for dataset 2 over conventional algorithms regarding " (a) Accuracy, (b) FDR, (c) FNR, (d) FPR, (e) NPV, and (f) Precision"

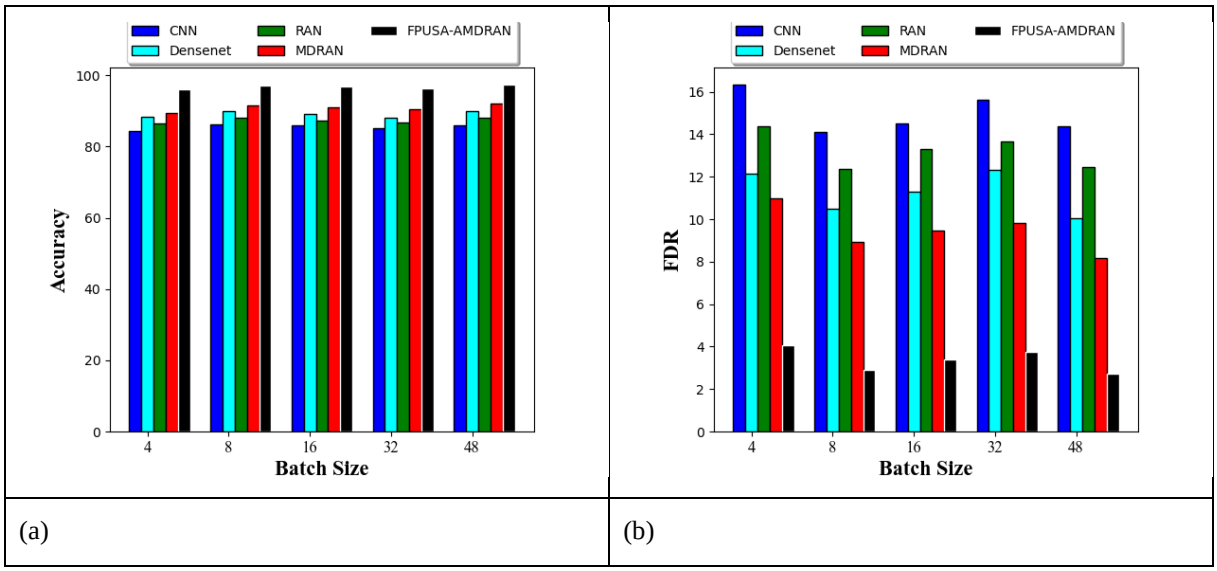

DOI: https://doi.org/10.54216/FPA.190217
Received: January 11, 2025 Revised: February 18, 2025 Accepted: March 06, 2025

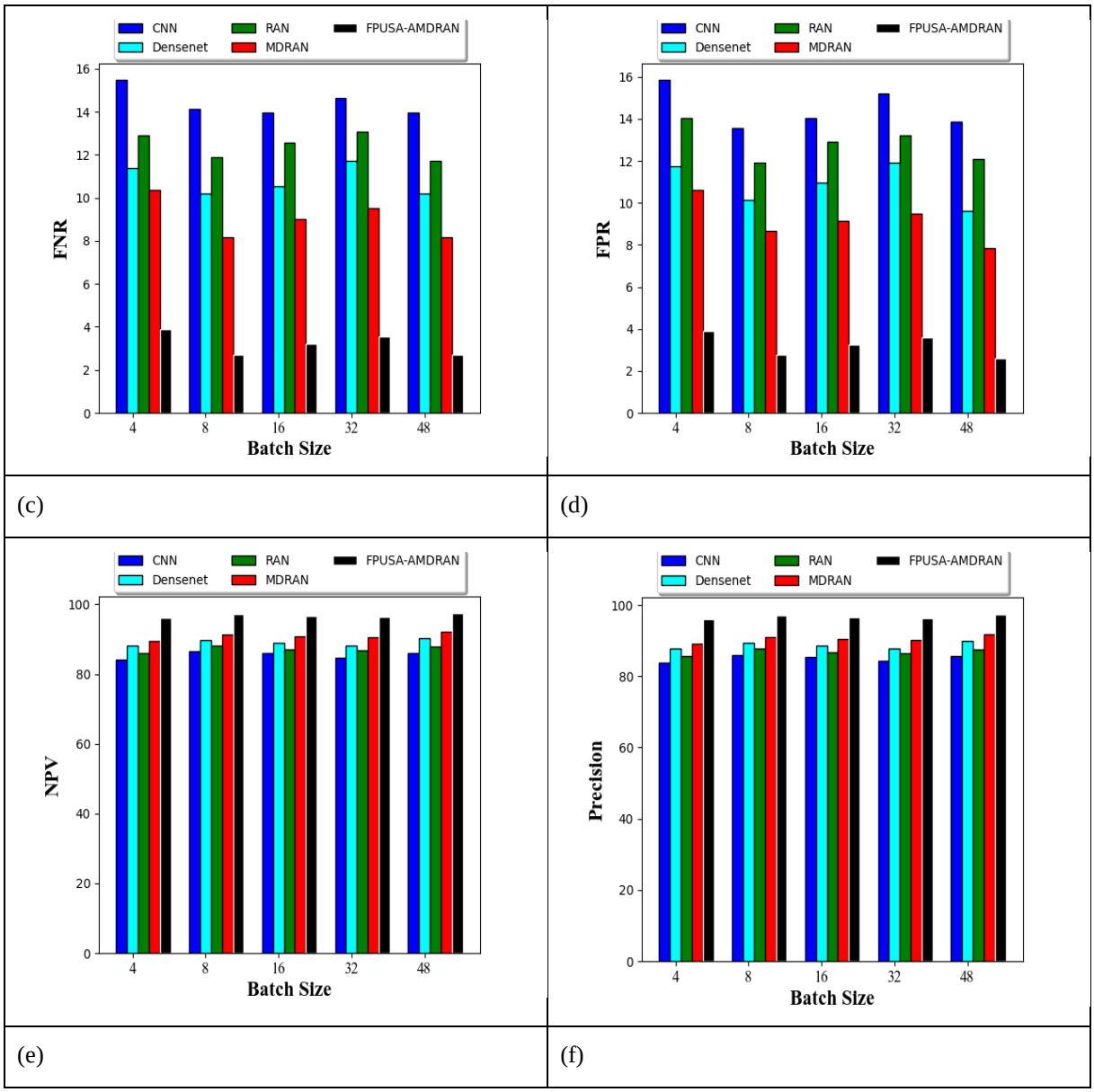

Figure 18. Performance analysis of designed ALL classification framework for dataset 2 over conventional classifiers regarding " (a) Accuracy, (b) FDR, (c) FNR, (d) FPR, (e) NPV, and (f) Precision"

6.9 Accuracy analysis of ALL classification process for dataset 1 and dataset 2

The accuracy estimation of ALL classification framework is displayed in Table III and Table IV for two datasets. The evaluation is conducted with the support of K-fold values such as 1,2,3,4, and 5 and by employing the accuracy factor. The K-fold-based analysis helps to ensure that the ALL classification process achieves higher accuracy and lower error rates than the traditional models. When focussing on the 5th k-fold value in Table III, the presented ALL classification process's accuracy is maximized by 11.38% of TFMOA-AMDRAN, 5.87% of CSO-AMDRAN, 7.84% of ZOA-AMDRAN, and 9.75% of SEO-AMDRAN respectively. Thus, it has been illustrated that the designed ALL classification process attained maximum accuracy rates than the traditional models.

DOI: https://doi.org/10.54216/FPA.190217
Received: January 11, 2025 Revised: February 18, 2025 Accepted: March 06, 2025

Table 3: Accuracy Analysis of ALL Classification Process for Dataset1 over Existing Algorithms and Classifiers

Algorithm comparison					
Terms	**TFMOA-AMDRAN [18]**	**CSO-AMDRAN [19]**	**ZOA-AMDRAN [20]**	**SEO-AMDRAN [16]**	**FPUSA-AMDRAN**
1	83.25	89	86.83333333	85.16666667	94.16666667
2	85.58333333	90.58333333	89.08333333	86.91666667	96.41666667
3	84.83333333	90.16666667	88.25	86.75	95.58333333
4	84.33333333	89.58333333	88.08333333	86.16666667	95
5	85.58333333	90.91666667	89	87.16666667	96.58333333
Classifier comparison					
Terms	**CNN [21]**	**Densenet [22]**	**RAN [17]**	**MDRAN [17] [23]**	**AMDRAN**
1	84.25	87.91666667	86.33333333	89.58333333	94.16666667
2	86.5	90.25	88.08333333	91.83333333	96.41666667
3	85.75	89.33333333	87.5	90.91666667	95.58333333
4	85.16666667	88.41666667	87	90.33333333	95
5	86.08333333	90.08333333	88.58333333	92.25	96.58333333

Table 4: Accuracy Analysis of ALL Classification Process for Dataset2 over Existing Algorithms and Classifiers

Algorithm comparison					
Terms	**TFMOA-AMDRAN [18]**	**CSO-AMDRAN [19]**	**ZOA-AMDRAN [20]**	**SEO-AMDRAN [16]**	**FPUSA-AMDRAN**
1	83.25	88.66666667	87.33333333	85	96.08333333
2	85.75	90.75	89.33333333	87.58333333	97.25
3	84.75	90	88.08333333	86.66666667	96.75
4	84.08333333	89.83333333	87.33333333	85.66666667	96.41666667
5	85.58333333	91.16666667	89.25	87.16666667	97.33333333
Classifier comparison					
Terms	**CNN [21]**	**Densenet [22]**	**RAN [17]**	**MDRAN [17] [23]**	**AMDRAN**
1	84.33333333	88.41666667	86.5	89.5	96.08333333

DOI: https://doi.org/10.54216/FPA.190217
Received: January 11, 2025 Revised: February 18, 2025 Accepted: March 06, 2025

2	86.16666667	89.83333333	88.08333333	91.58333333	97.25
3	86	89.25	87.25	90.91666667	96.75
4	85.08333333	88.16666667	86.83333333	90.5	96.41666667
5	86.08333333	90.08333333	88.08333333	92	97.33333333

7. Conclusion

This work has explored an efficient and automated ALL diagnosis process with the presence of deep learning strategies. From the available data sources, the significant images were aggregated. Next, the images were subjected to the segmentation process, where the OTRUnet+ technique assisted in segmenting the abnormalities. In order to enhance the efficacy of the segmentation operation, the FPUSA was introduced. Subsequently, the segmented images were subjected to the AMDRAN approach, where ALL is diagnosed. Here also, to enrich the functionality rates of the classification process the FPUSA was employed by optimizing the parameters of AMDRAN. At last, detailed experiments were carried out to verify the effectiveness of the system. When focussing on the 48th batch size in second dataset, the FPR of the developed ALL classification approach was minimized by 58.1% of TFMOA-AMDRAN, 34.5% of CSO-AMDRAN, 36.3% of ZOA-AMDRAN, and 52.7% of SEO-AMDRAN respectively. From the experiments, it has been confirmed that the implemented ALL classification task attained its superior qualities over traditional techniques. In the future, the recommended work will be expanded to classify numerous categories of WBCs and synergize genetic data and images to produce a high-potential ensemble technique. Moreover, the recommended work will be strengthened to classify the ALL by re-training the technique with very little effort.

References

[1] J. L. Diaz Resendiz, V. Ponomaryov, R. Reyes Reyes, and S. Sadovnychiy, "Explainable CAD System for Classification of Acute Lymphoblastic Leukemia Based on a Robust White Blood Cell Segmentation," *Cancers*, vol. 15, no. 3376, 2023.

[2] S. Alagu, A. P. N, and B. B. K, "Automatic detection of acute lymphoblastic leukemia using UNET based segmentation and statistical analysis of fused deep features," *Appl. Artif. Intell.*, vol. 35, pp. 1952–1969, 2021.

[3] S. Anwar and A. Alam, "A convolutional neural network–based learning approach to acute lymphoblastic leukemia detection with automated feature extraction," *Med. Biol. Eng. Comput.*, vol. 58, pp. 3113–3121, 2020.

[4] N. Sampathila et al., "Customized deep learning classifier for detection of acute lymphoblastic leukemia using blood smear images," *Healthcare*, vol. 10, no. 10, 2022.

[5] U. Saeed et al., "DeepLeukNet—A CNN based microscopy adaptation model for acute lymphoblastic leukemia classification," *Multimed. Tools Appl.*, vol. 83, pp. 21019–21043, 2024.

[6] M. Jawahar, H. Sharen, and A. H. Gandomi, "ALNett: A cluster layer deep convolutional neural network for acute lymphoblastic leukemia classification," *Comput. Biol. Med.*, vol. 148, no. 105894, 2022.

[7] M. Zakir Ullah et al., "An attention-based convolutional neural network for acute lymphoblastic leukemia classification," *Appl. Sci.*, vol. 11, no. 10662, 2021.

[8] L. F. Rodrigues, A. R. Backes, B. A. N. Travençolo, and G. M. B. de Oliveira, "Optimizing a deep residual neural network with genetic algorithm for acute lymphoblastic leukemia classification," *J. Digit. Imaging*, vol. 35, pp. 623–637, 2022.

[9] E. Özbay, F. A. Özbay, and F. S. Gharehchopogh, "Peripheral blood smear images classification for acute lymphoblastic leukemia diagnosis with an improved convolutional neural network," *J. Bionic Eng.*, pp. 1–17, 2023.

DOI: https://doi.org/10.54216/FPA.190217
Received: January 11, 2025 Revised: February 18, 2025 Accepted: March 06, 2025

[10] P. K. Das and S. Meher, "An efficient deep convolutional neural network based detection and classification of acute lymphoblastic leukemia," *Expert Syst. Appl.*, vol. 183, no. 115311, 2021.

[11] S. I. Ur Rahman et al., "Efficient segmentation of lymphoblast in acute lymphocytic leukemia," *Sci. Program.*, pp. 1–7, 2021.

[12] A. Abhishek, R. K. Jha, R. Sinha, and K. Jha, "Automated classification of acute leukemia on a heterogeneous dataset using machine learning and deep learning techniques," *Biomed. Signal Process. Control*, vol. 72, no. 103341, 2022.

[13] C. Mondal et al., "Acute lymphoblastic leukemia detection from microscopic images using weighted ensemble of convolutional neural networks," *arXiv preprint*, 2021.

[14] G. Atteia, A. A. Alhussan, and N. A. Samee, "BO-ALLCNN: Bayesian-based optimized CNN for acute lymphoblastic leukemia detection in microscopic blood smear images," *Sensors*, vol. 22, no. 5520, 2022.

[15] S. Ramaneswaran, K. Srinivasan, P. D. R. Vincent, and C. Y. Chang, "Hybrid inception v3 XGBoost model for acute lymphoblastic leukemia classification," *Comput. Math. Methods Med.*, pp. 1–10, 2021.

[16] A. M. Fathollahi-Fard, M. Hajiaghaei-Keshteli, and R. Tavakkoli-Moghaddam, "The Social Engineering Optimizer (SEO)," *Eng. Appl. Artif. Intell.*, vol. 72, pp. 267–293, Jun. 2018.

[17] M. M. Qanbar and S. Tasdemir, "Detection of malaria diseases with residual attention network," *Int. J. Intell. Syst. Appl. Eng.*, vol. 7, pp. 238–244, 2019.

[18] A. V. Panteleev and A. A. Kolessa, "Application of the tomtit flock metaheuristic optimization algorithm to the optimal discrete-time deterministic dynamical control problem," *Algorithms*, vol. 15, no. 301, 2022.

[19] H. A. Akkar and S. A. Salman, "Cicada Swarm Optimization: A New Method for Optimizing Persistent Problems," *Int. J. Intell. Eng. Syst.*, vol. 13, 2020.

[20] E. Trojovská, M. Dehghani, and P. Trojovský, "Zebra optimization algorithm: A new bio-inspired optimization algorithm for solving optimization algorithm," *IEEE Access*, vol. 10, pp. 49445–49473, 2022.

[21] V. D. A. Kumar et al., "An effective method for predicting postpartum haemorrhage using deep learning techniques," *Multimed. Tools Appl.*, 2022. Available: https://doi.org/10.1007/s11042-021-11622-4.

[22] E. H. Houssein et al., "Using deep DenseNet with cyclical learning rate to classify leukocytes for leukemia identification," *Front. Oncol.*, vol. 13, no. 1230434, 2023.

[23] N. Takahashi and Y. Mitsufuji, "Densely connected multi-dilated convolutional networks for dense prediction tasks," in *Proc. IEEE/CVF Conf. Comput. Vis. Pattern Recognit.*, pp. 993–1002, 2021.

[24] A. H. Alharbi et al., "Segmentation and classification of white blood cells using the UNet," *Contrast Media Mol. Imaging*, 2022.

[25] Y. Xu, S. Hou, X. Wang, D. Li, and L. Lu, "A medical image segmentation method based on improved UNet 3+ network," *Diagnostics*, vol. 13, no. 576, 2023.

[26] J. Chen et al., "Transunet: Transformers make strong encoders for medical image segmentation," *arXiv preprint*, 2021.

DOI: https://doi.org/10.54216/FPA.190217
Received: January 11, 2025 Revised: February 18, 2025 Accepted: March 06, 2025